

On weakly turbulent scaling of wind sea in simulations of fetch-limited growth

ELODIE GAGNAIRE-RENOU^{1,2,3,†}, MICHEL BENOIT^{1,2}
AND SERGEI I. BADULIN^{4,5}

¹Saint-Venant Laboratory for Hydraulics, Université Paris Est (joint research unit EDF R&D, CETMEF, Ecole des Ponts Paris Tech), c/o EDF R&D, 6 quai Watier, BP 49, 78401 Chatou, France

²Laboratoire National d'Hydraulique et Environnement (LNHE), EDF R&D, 6 quai Watier, BP 49, 78401 Chatou, France

³Laboratoire de Sondages Electromagnétiques de l'Environnement Terrestre (LSEET), Université du Sud Toulon-Var, BP 132, 83957 La Garde, France

⁴P.P. Shirshov Institute of Oceanology of Russian Academy of Sciences, 36, Nakhimovskii pr., Moscow 117997, Russia

⁵Laboratory of Nonlinear Wave Processes, Novosibirsk State University, 630090, Novosibirsk, Russia

(Received 30 September 2009; revised 17 September 2010; accepted 17 September 2010;
first published online 5 January 2011)

Extensive numerical simulations of fetch-limited growth of wind-driven waves are analysed within two approaches: a ‘traditional’ wind-speed scaling first proposed by Kitaigorodskii (*Bull. Acad. Sci. USSR, Geophys. Ser., Engl. Transl.*, vol. N1, 1962, p. 105) in the early 1960s and an alternative weakly turbulent scaling developed recently by Badulin *et al.* (*J. Fluid Mech.* **591**, 2007, 339–378). The latter one uses spectral fluxes of wave energy, momentum and action as physical scales of the problem and allows for advanced qualitative and quantitative analysis of wind-wave growth and features of air–sea interaction. In contrast, the traditional approach is shown to be descriptive rather than proactive. Numerical simulations are conducted on the basis of the Hasselmann kinetic equation for deep-water waves in a wide range of wind speeds from 5 to 30 m s⁻¹ and for the ideal case of fetch-limited growth: permanent wind blowing perpendicularly to a straight coastline. Two different wave input functions, S_{in} , and two methods for calculating the nonlinear transfer term S_{nl} (Gaussian quadrature method, or GQM, a quasi-exact method based on the use of Gaussian quadratures, and the discrete interaction approximation, or DIA) are used in the simulations. Comparison of the corresponding results firstly shows the relevance of the analysis of wind-wave growth in terms of the proposed weakly turbulent scaling, and secondly, allows us to highlight some critical points in the modelling of wind-generated waves. Three stages of wind-wave development corresponding to qualitatively different balance of the source terms, S_{in} , S_{diss} and S_{nl} , are identified: initial growth, growing sea and fully developed sea. Validity of the asymptotic weakly turbulent approach for the stage of growing wind sea is determined by the dominance of nonlinear transfers, which results in a rigid link between spectral fluxes and wave energy. This stage of self-similar growth is investigated in detail and presented as a consequence of three sub-stages of qualitatively different coupling of air flow and growing wind waves. The key self-similarity parameter of the asymptotic theory is estimated to be $\alpha_{ss} = 0.68 \pm 0.1$.

† Email address for correspondence: elodie.gagnaire-renou@edf.fr

Further prospects of wind-wave modelling in the context of the presented weakly turbulent scaling are discussed.

Key words: surface gravity waves, waves/free-surface flows, wind-wave interactions

1. Introduction

The Hasselmann kinetic equation is the basic theoretical model for statistical description of surface gravity waves. First derived by Hasselmann (1962) for modelling the evolution of weakly nonlinear free waves (with no wind input nor dissipation), it was further generalized to the case of wind waves and became the core of all the modern spectral forecasting models of wind-driven seas (e.g. WAMDI Group 1988). The extension of the original Hasselmann equation is written as follows in the absence of ambient current:

$$\frac{\partial N_{\mathbf{k}}}{\partial t} + \nabla_{\mathbf{k}} \omega_{\mathbf{k}} \nabla_{\mathbf{r}} N_{\mathbf{k}} = S_{in} [N_{\mathbf{k}}] + S_{diss} [N_{\mathbf{k}}] + S_{nl} [N_{\mathbf{k}}], \quad (1.1)$$

where $N(\mathbf{k})$ is the two-dimensional wave action spectral density, defined as $N(\mathbf{k}) = F(\mathbf{k})/\omega(\mathbf{k})$, and $F(\mathbf{k})$ is the two-dimensional variance spectral density. The variable \mathbf{k} is the wavenumber vector, related to the intrinsic frequency ω through the linear dispersion relationship for gravity water waves,

$$\omega^2(\mathbf{k}) = g|\mathbf{k}| \tanh(|\mathbf{k}|d), \quad (1.2)$$

with d being the water depth. Terms on the right-hand side of (1.1) describe wave input by wind forcing S_{in} , wave dissipation S_{diss} dealing with a number of physical mechanisms and nonlinear transfer due to resonant four-wave interactions, S_{nl} . In this study, deep-water conditions are considered ($|\mathbf{k}|d \gg 1$), so that (1.2) reduces to $\omega^2 = g|\mathbf{k}|$.

Vector quantity $\mathbf{M}(\mathbf{k}) = \mathbf{k}N(\mathbf{k})$, known as the wave momentum spectral density, can be introduced straightforwardly. The three physical quantities, $N(\mathbf{k})$, $F(\mathbf{k})$ and $\mathbf{M}(\mathbf{k})$, are equally important for the statistical description of waves being associated with conservation laws of the kinetic equation in the absence of wave input and dissipation (i.e. $S_{in} \equiv 0$, $S_{diss} \equiv 0$ in (1.1)). Strictly speaking, functions $N(\mathbf{k})$, $F(\mathbf{k})$, $\mathbf{M}(\mathbf{k})$ for weakly nonlinear waves are related to their ‘linear’ counterparts by a quadratic transformation (see Krasitskii 1994, Zakharov 1999 and Badulin *et al.* 2005) and equivalence of the ‘linear’ and ‘weakly nonlinear’ functions can be accepted as an approximation, which is valid only for deep-water waves.

In this paper, we follow a conventional statistical approach for wind waves (Zakharov 1999), passing over a number of questions related to the validity of the kinetic equation (1.1), the role of non-resonant interactions (e.g. Annenkov & Shrira 2006), the effect of long- and short-wave interactions (see Phillips 1981), etc. All these questions remain very important for studying particular mechanisms of wind-wave growth. The goal of the paper is rather to present a general vision, which considers wind-wave growth as a result of three main physical processes: nonlinear transfer, wave generation and wave dissipation. We show that some general features of wind-wave growth do exist and can be revealed independently of ‘details’ of wind-wave interaction mechanisms.

An attempt to generalize the problem of wind-wave growth has been made by Kitaigorodskii (1962) (see also Kitaigorodskii 1983); the same year the kinetic

equation was established by Hasselmann. Friction velocity of turbulent wind, $u_* = \sqrt{\tau_s/\rho_a}$ (τ_s is the surface shear stress and ρ_a the air density), was proposed as a key physical scale of growing wind waves. This scaling together with scaling by wind speed U_h at a reference height h above the mean sea level have been widely used in wind-wave studies for almost 50 years. They are often referred to as ‘Kitaigorodskii scalings’ or ‘Kitaigorodskii similarity approaches’. Although these scalings can be convenient as wind speed is a key measurable characteristic of wind-wave interaction, they ignore the complexity of wind effects on waves such as gustiness, air-flow stratification, etc., and thus imply heavy idealization of the problem.

It should be noted that Kitaigorodskii (1962), in his similarity approach, does not rely only on the wind-speed scaling. In his detailed physical scheme (see figure 5 in Kitaigorodskii 1962), the wave energy dissipation rate, ε_{max} , was considered as a scale of mechanisms similar to Kolmogorov’s cascading in hydrodynamic turbulence. Nowadays, this naive ‘too direct’ analogy with Kolmogorov’s turbulence can be seen as a precursor of later advances of the weak turbulence theory for water waves (see Zakharov 1966, Zakharov & Filonenko 1966 and Zakharov, Falkovich & Lvov 1992).

In this paper, we aim at extending our understanding of wind-wave growth by introducing a weakly turbulent scaling, based on spectral fluxes providing the nonlinear cascading. Recent studies by Badulin *et al.* (2005, 2007) have confirmed the leading role of nonlinear transfer and, as a result, pronounced features of self-similarity of growing wind seas. They proposed an asymptotic model which provides families of self-similar solutions and explicit asymptotic relationships that link integral wave energy $E = \int \omega(\mathbf{k})N(\mathbf{k}) d\mathbf{k}$, wave action $N = \int N(\mathbf{k}) d\mathbf{k}$ and wave momentum $M = \int \mathbf{k}N(\mathbf{k}) d\mathbf{k}$ with the corresponding spectral fluxes. These are what Badulin *et al.* (2007) called ‘weakly turbulent laws of wind-wave growth’.

The advantage of the asymptotic approach by Badulin *et al.* (2007) is that the nonlinear transfer term (collision integral S_{nl}) is known ‘from first principles’ and does not contain any free parameters. This is in contrast to our current knowledge of the terms S_{in} , S_{diss} , which relies heavily upon empirical dependences. Ocean-field experiments give no direct way to discriminate between wave generation or dissipation and to experimentally quantify the nonlinear transfer term S_{nl} which co-exists with S_{in} , S_{diss} (Plant 1982). To resolve this problem, heuristic or semi-empirical models for S_{in} , S_{diss} are widely used (e.g. the whitecapping mechanism by Hasselmann 1974) as workpieces for further parametrizing the observed wave input and dissipation. Experimental studies of S_{in} , S_{diss} have often been carried out for a quite narrow range of physical conditions (low winds, narrow range of wave scales, etc.) and the physical relevance of these heuristic models is generally not clear. The more recent parametrizations of S_{in} and S_{diss} are more physically based and use more parameters of the wave field (e.g. wave steepness or breaking threshold parametrization in Donelan *et al.* 2006, Young & Babanin 2006 and Filipot, Arduin & Babanin 2010). They may potentially be applied to a wider range of sea states. At the same time, they still remain empirically rather than theoretically based and cannot guarantee success of wind-wave modelling in general case.

Thus, the traditional wind-speed scaling of wind-wave growth raises questions, firstly because of the uncertainty of our knowledge of S_{in} , S_{diss} . Secondly, it reflects essential features of wind-wave coupling where wind speed is, evidently, important but it is just one of a number of physical parameters describing the coupling.

The goal of this paper is to show advantages of the weakly turbulent scaling as a proactive tool for developing wind-wave models. An extensive simulation of fetch-limited growth in the spirit of test beds for wind-wave forecasting models (e.g.

SWAMP Group 1985 and Komen *et al.* 1994) has been carried out and its results are analysed both within the traditional wind-speed scaling and the weakly turbulent approach. This analysis firstly allows us to identify essential physical properties of wind-wave growth and, secondly, to advance the understanding of everyday problems in wind-wave modelling: choice of models for S_{in} , S_{diss} , adequacy of approximate methods for calculating S_{nl} . Mature seas are also discussed as a limiting case of growing seas.

In §2, we present the set-up of our numerical experiments. Conditions and parameters of the simulations are reported. The chosen functions for S_{in} and S_{diss} are basically described, as well as the numerical methods for computing S_{nl} . Section 3 introduces conventional wind-speed scaling and an alternative one using results of the theory of weak turbulence (Zakharov *et al.* 1992). An asymptotic weakly turbulent model, the so-called split-balance model (Badulin *et al.* 2007), provides families of non-stationary and non-homogeneous self-similar solutions with rigid links of spectral fluxes to spectral magnitudes quite similarly to the classic stationary Kolmogorov–Zakharov solutions (Zakharov 1966; Zakharov & Filonenko 1966; Zakharov & Zaslavsky 1982*a*). Three reference cases of the self-similar wave growth are of special interest: they correspond to constant fluxes of wave momentum, energy or wave action. These cases were derived long ago (Toba 1972; Hasselmann *et al.* 1976; Zakharov & Zaslavsky 1983*b*) from very different theoretical and experimental premises. The presented weakly turbulent approach allows us to associate these reference cases with qualitatively different stages of wave growth. In §4, results of numerical simulations are described both in terms of wind-speed scaling and in terms of spectral flux weakly turbulent scaling. Different stages of wave development from initial growth to the fully developed (mature) sea are delimited qualitatively and quantitatively. The stage of growing wind sea described by the asymptotic weakly turbulent theory is detailed as a consequence of qualitatively different sub-stages of air–sea coupling based on the reference cases (Toba 1972; Hasselmann *et al.* 1976; Zakharov & Zaslavsky 1983*b*) mentioned above. Section 5 closes the paper with discussions and conclusions.

2. Numerical model of fetch-limited growth

In this section, we describe the set-up of our numerical studies of fetch-limited growth. Generally, we follow similar works on wind-wave modelling (Komen, Hasselmann & Hasselmann 1984; Komen *et al.* 1994), drawing attention to possible coupling and, as our results show, the most realistic composition of nonlinear transfer, wave input and dissipation terms. Using different approaches (i.e. models or methods) for the wave input function S_{in} and for the nonlinear transfer term S_{nl} , we are trying to understand how our approximations and empirical parametrizations can affect the resulting evolution of wave spectrum. The conceptual difficulty of such a study essentially lies in the nonlinear physics of sea state evolution: benefits and disadvantages of these approaches cannot be assessed for each of the terms independently. Interdependence of wave input, dissipation and nonlinear transfer requires a certain coordination of the approaches to ensure basic features of wind-wave physics.

2.1. Conditions and parameters of simulation

The idea of the numerical set-up is to reproduce wave-spectrum evolution under some standard conditions. We let wind blow offshore normally to a straight coast ($\theta_u = 0$). The 10 m wind speeds U_{10} range from 5 to 30 m s⁻¹. (We considered four

standard values: $U_{10} = 5, 10, 20, 30 \text{ m s}^{-1}$.) The wave field is assumed homogeneous in the longshore direction.

The Hasselmann equation (1.1) is solved both in space and time to guarantee physically relevant stationary solutions developing in the offshore direction. The simulation parameters were selected so as to maintain the same dimensionless parameters (non-dimensional fetch $\chi = xg/U_{10}^2$, non-dimensional frequency $\tilde{f} = fU_{10}/g$ and non-dimensional time $\tau = gt/U_{10}$) in each simulation.

The spatial grid comprises 121 nodes, which are in geometric progression with increasing Δx from the shore line ($\Delta x_{n+1}/\Delta x_n = 1.068$; $\Delta x_1 = 6.25 \text{ m}$ for $U_{10} = 5 \text{ m s}^{-1}$, while $\Delta x_1 = 225 \text{ m}$ for $U_{10} = 30 \text{ m s}^{-1}$). The maximal fetch x_{max} , corresponding to non-dimensional fetch $\chi_{max} = 10^5$ in each simulation, was chosen to be sufficiently long to reach a mature sea state. The very existence of this state is a specific issue (see Komen *et al.* 1984) that we discuss below.

The discrete frequency-direction grid is composed of 51 frequencies with geometric progression ($f_{n+1}/f_n = 1.071$) and 36 directions with a constant spacing of 10° ($\theta_{m+1} - \theta_m = 10^\circ$). For wind speeds $U_{10} = 5, 10, 20, 30 \text{ m s}^{-1}$, the corresponding lowest and highest frequencies are $f_1 = 0.16, 0.08, 0.04, 0.027 \text{ Hz}$ and $f_{51} = 5, 2.5, 1.25, 0.83 \text{ Hz}$, respectively. These resolutions are adequate for the problem discussed, as has been shown by Komatsu & Masuda (1996). Additional tests have been carried out within our approach with finer frequency and directional resolutions (from 51 to 128 frequencies and up to 72 directions, respectively). Results are only marginally affected by the finer resolutions, while CPU time increases dramatically.

The initial wave spectrum (at $t = 0$) is set to be plain zero (see (A 6) of Appendix A). Time integration of the source terms is performed with a semi-implicit scheme (WAMDI Group 1988) with a constant time step. ($\Delta t = 5, 10, 20, 30 \text{ s}$ for the corresponding wind speeds, $U_{10} = 5, 10, 20, 30 \text{ m s}^{-1}$.) Results are given at non-dimensional time $\tau_f = gt_f/U_{10} \approx 6.36 \times 10^4$ (corresponding to 9, 18, 36 and 54 h of physical time, respectively) as corresponding to quasi-stationary state and, thus, to fetch-limited growth.

In these simulations, we used the wave growth limiter corresponding to the modified WAM-Cycle 4 expression of Hersbach & Janssen (1999):

$$|\Delta F|_{max} = 3.0 \times 10^{-7} g \max(u_*, gf_{PM}^*/f) f^{-4} f_{51} \Delta t, \quad (2.1)$$

where $f_{PM}^* = 5.6 \times 10^{-3}$ is the non-dimensional Pierson–Moskowitz frequency. Benoit (2006) analysed the influence of different wave growth limiters on spectrum development, and recommended the use of (2.1) when such a limiter is necessary (for instance, when using a large static time step).

In the wave model, the high-frequency range of the spectrum (above a given frequency f_d) is introduced in a standard way as power-like extrapolation $F(f, \theta) \propto f^{-m}$, with $m = 4$. The diagnostic frequency f_d is set as follows:

$$f_d = \min[f_{51}; \max(4f_{PM}, 2.5\bar{f})], \quad (2.2)$$

where the mean frequency \bar{f} is given by

$$\bar{f} = m_0 \left(\int_0^{+\infty} \int_{-\pi}^{\pi} f^{-1} F(f, \theta) df d\theta \right)^{-1}, \quad (2.3)$$

with

$$m_0 = \int_0^{+\infty} \int_{-\pi}^{\pi} F(f, \theta) df d\theta = E. \quad (2.4)$$

Such a diagnostic high-frequency tail is usually used in simulations of spectral evolution to compensate the lack of physics of S_{in} and S_{diss} in the high-frequency part of the spectrum or to reduce the computational time. The inclusion of a high-frequency diagnostic tail and the particular choice of exponent m and frequency f_d affect the whole evolution of the spectrum (e.g. Banner & Young 1994 and Gagnaire-Renou, Benoit & Forget 2010). In particular, the high-frequency diagnostic tail influences the wave input and dissipation terms when parametrizations for S_{in} and S_{diss} depend on wave spectrum. Thus, special care should be taken to discriminate between the wave input and dissipation terms themselves and artefacts due to choice of the diagnostic tail. Note that we follow standard set-up for the modelling of wind-wave spectrum when introducing a diagnostic tail (e.g. WAMDI Group 1988).

2.2. Two formulations of the wind input term

A large number of parametrizations have been proposed for modelling the wind input term S_{in} (e.g. Stewart 1974; Snyder *et al.* 1981; Plant 1982; Hsiao & Shemdin 1983; Donelan & Pierson Jr 1987; Janssen 1989; Janssen 1991). In fact, all these parametrizations can be written as a quasi-linear form:

$$S_{in}^{(F)} = \omega\beta(u_*/C_{ph}, \theta, u_1, \dots)F(f, \theta). \quad (2.5)$$

The key argument of the non-dimensional increment β is the ratio of wave phase velocity C_{ph} to friction velocity u_* (or a reference wind speed U_{10}): C_{ph}/u_* , the so-called wave age of a particular wave component. Wave harmonic generation is assumed to occur if ratio C_{ph}/u_* is below a certain threshold, quite similarly to the effect of Cherenkov radiation well known in many domains of modern physics (i.e. light–particle interaction, wave generation by bodies at supersonic speeds, etc.). Only waves propagating slower than this threshold (say, slower than wind speed at height U_{10}) can be generated or amplified, and waves propagating faster than this threshold, the so-called old waves, are not affected, or even damped by the wind. Other arguments u_i are introduced in β to describe the variety of additional physical effects in wind-wave coupling.

Note that S_{in} was defined in (1.1) in terms of wave action $N(\mathbf{k})$. In (2.5), wave input is introduced in terms of the variance spectrum $F(f, \theta)$. For convenience, superscript for S_{in} (and other source–sink terms) is omitted in the following.

In our study, we consider two input terms S_{in} , which are usually implemented as options in the most recent third-generation (3G) models (e.g. WAM, WAMDI Group 1988, Komen *et al.* 1994; Wavewatch-III, Tolman 1991, 2002; SWAN, Booij *et al.* 1999; TOMAWAC, Benoit *et al.* 1996): the model by Snyder *et al.* (1981), used in WAM-Cycle 3, and the model by Janssen (1989, 1991), as implemented in WAM-Cycle 4. The corresponding expressions are given in Appendix A.

An important point of our study is that the total wave input (integral in wave scales) is a key quantity of wind-wave growth. We show below that the wind-wave growth is determined by this basic quantity of air–sea interaction rather than by particular dependence of wave input on wave frequency. Even at first glance, the wave input parametrizations we use can give a quite different integral wave input (see figure 11 in Appendix A). As a consequence, different wave growths due to these input functions are to be expected because of this simple (but not trivial) fact.

2.3. Wave dissipation: whitecapping by Hasselmann (1974)

Wave dissipation has long been and may still be regarded as the most poorly understood term in the kinetic equation (1.1). The quasi-linear parametrization of

the whitecapping mechanism by Hasselmann (1974) is still implemented in most of the wind-wave forecasting models. However, recent observations (see e.g. Ardhuin, Chapron & Collard 2009) have led to new developments, and massive efforts are being undertaken to extend our knowledge of this physical mechanism. The threshold and cumulative behaviours of the dissipation have been discussed by, e.g., Banner, Babanin & Young (2000) and Young & Babanin (2006). Saturation-based parametrizations are addressed in recent works of, e.g., Alves & Banner (2003), Van der Westhuysen, Zijlema & Battjes (2007) and Ardhuin *et al.* (2008), to be used in operational models of wave forecasting while essentially nonlinear parametrizations of the term S_{diss} (e.g. Phillips 1985 and Donelan & Pierson Jr 1987) are treated predominantly in the context of research models. Current work by Filipot *et al.* (2010) intend to unify deep- and shallow-water wave breaking.

Some problems of the original whitecapping parametrization were demonstrated by Komen *et al.* (1984) for the balance of fully developed wind-driven sea. Nowadays, spectral wind-wave models use this parametrization in the following form:

$$S_{diss}(f, \theta) = -\frac{C_{diss}}{g^p} \bar{\omega}^{2p+1} m_0^{p/2} \left[\delta \left(\frac{\omega}{\bar{\omega}} \right)^2 + (1 - \delta) \left(\frac{\omega}{\bar{\omega}} \right)^4 \right] F(f, \theta), \quad (2.6)$$

where $\bar{\omega}$ is defined by $\bar{\omega} = 2\pi\bar{f}$ (see (2.3)). $C_{diss} = 4.5$ and $\delta = 0.5$ are default values in the WAM-Cycle 4 model (Günther, Hasselmann & Janssen 1992; Komen *et al.* 1994). The exponent $p = 4$ is usually used in (2.6). Zakharov *et al.* (2007) and Korotkevich *et al.* (2008) have recently found that the whitecapping dissipation is overestimated in the WAM-Cycle 3 and WAM-Cycle 4 models. They propose the dissipation term (2.6) with $C_{diss} = 0.11$, $\delta = 0$ and $p = 12$. The key message of such revision is a high exponent p that models threshold-like dependence of dissipation on wave steepness, $\varepsilon = \bar{\omega} \sqrt{m_0}/g$.

In our study, we follow WAM-Cycle 4 formula for S_{diss} (2.6) with standard parameters given above. Effects of the parameters as well as alternative formulations for the dissipation term are subjects of further studies.

2.4. Modelling the nonlinear transfer term S_{nl}

The Hasselmann equation (1.1) presupposes that the nonlinear transfer term S_{nl} plays a leading role in the evolution of the wave spectrum. This leading role of the nonlinear transfer for wind-driven seas was demonstrated both theoretically (Young & Van Vledder 1993; Badulin *et al.* 2005; Badulin *et al.* 2008b) and experimentally (Pettersson 2004; Young 2006). This is in conceptual contradiction with models that consider wave generation and dissipation as main constituents of the wind-sea balance, and assume that input and dissipation terms solely determine the shape of the wave spectrum and its evolution in space and time (e.g. Phillips 1985; Hara & Belcher 2002).

The motivation to simplify the nonlinear transfer term S_{nl} , or even remove it, comes from the difficulties associated with a precise calculation of this term, which is expressed as a sixfold integral on wavenumber vector components:

$$S_{nl} [N_k] = \int_{\mathbf{k}_1} \int_{\mathbf{k}_2} \int_{\mathbf{k}_3} G(\mathbf{k}, \mathbf{k}_1, \mathbf{k}_2, \mathbf{k}_3) \{N_2 N_3 (N + N_1) - N N_1 (N_2 + N_3)\} \\ \times \delta(\mathbf{k} + \mathbf{k}_1 - \mathbf{k}_2 - \mathbf{k}_3) \delta(\omega + \omega_1 - \omega_2 - \omega_3) d\mathbf{k}_1 d\mathbf{k}_2 d\mathbf{k}_3. \quad (2.7)$$

Functions N_k are generally strongly localized in wave vector space. The kernel $G(\mathbf{k}, \mathbf{k}_1, \mathbf{k}_2, \mathbf{k}_3)$ (see e.g. Badulin *et al.* 2005, for a collection of possible representations) grows rapidly with wave vector (as $|\mathbf{k}|^6$) and δ -functions contour the subspace of

resonant quadruplets

$$\left. \begin{aligned} \mathbf{k} + \mathbf{k}_1 &= \mathbf{k}_2 + \mathbf{k}_3, \\ \omega + \omega_1 &= \omega_2 + \omega_3. \end{aligned} \right\} \quad (2.8)$$

A number of algorithms for exact evaluation of collision integral S_{nl} has been proposed starting with the Webb (1978) method, referred to as WRT (Tracy & Resio 1982), which was further developed in a number of works; see Resio & Perrie (1991), Pushkarev, Resio & Zakharov (2003) and van Vledder (2006). The EXACT-NL code by Hasselmann & Hasselmann (1981, 1985) was the first that was applied for burning questions of wind-sea physics (Komen *et al.* 1984). Methods by Masuda (1986), Komatsu & Masuda (1996) and then by Hashimoto, Tsuruya & Nakagawa (1998), Polnikov (1990) and, finally, by Lavrenov (2001) can be considered as versions of the Hasselmann method with particular transformations of variables and different methods for processing singularities in the integrands.

Simplified methods are usually used in 3G wave models. Among them, the discrete interaction approximation (DIA) method (Hasselmann *et al.* 1985) has been the most frequently employed since the WAM model was proposed (WAMDI Group 1988). The multiple DIA (MDIA; e.g. Tolman 2004) is an extension of the original DIA, and considers various quadruplet configurations. These methods can give very reasonable results in simple situations, but they result in significant qualitative and quantitative differences (e.g. in the situation of abrupt changes of wind direction: Young *et al.* 1987) when compared with exact methods, which makes their use questionable in the general case.

Benoit (2005) reviewed and compared several possible improvements or alternative techniques to obtain higher accuracy in the evaluation of (2.7) while keeping acceptable CPU time. He found that the integration technique proposed by Lavrenov (2001), called the Gaussian quadrature method (GQM), can give adequate results regarding both precision and CPU time. The GQM is based on the use of Gaussian quadratures adapted to the singularities that appear in the course of the manipulation of the kinetic integral (2.7). Like all the exact methods mentioned above, it can be simplified using a coarser resolution and/or a reduced integration range. Various resolutions of GQM and their effect on spectral shapes have been investigated in detail by Benoit & Gagnaire-Renou (2007). Indications about CPU times can be found in Appendix B.

As an illustration, figure 1 shows S_{nl} terms given by DIA and MDIA as proposed by Tolman (2004) and by GQM with three different resolutions, for a given JONSWAP-like spectrum. ‘Fine’ GQM resolution with 26, 16 and 12 points (denoted (26,16,12) in short) for the first, second and third components of integration (after suppressing the Dirac functions in 2.7) is considered as ‘true’ nonlinear transfer term and is given by a solid line in both panels of figure 1. ‘Medium’ (14,8,8) and ‘rough’ (11,6,6) resolutions show some deviations from the ‘true’ curve of the fine resolution, especially in the high-frequency range. Differences between fine and medium resolutions are small, and almost invisible near the spectral peak, which confirms the good convergence of the method when increasing its resolution. On the basis of these results, we accept GQM with medium resolution as a regular one for the present study. Fine resolution has been used in some cases only to control the accuracy of simulations.

The pronounced difference between the DIA and the reference GQM-fine curves does not require detailed comments. One can note several positive lobes of the DIA curve and a very deep negative lobe shifted towards higher frequencies relative to the reference curve (see Benoit 2005 and Cavaleri *et al.* 2007 for further comparisons). The

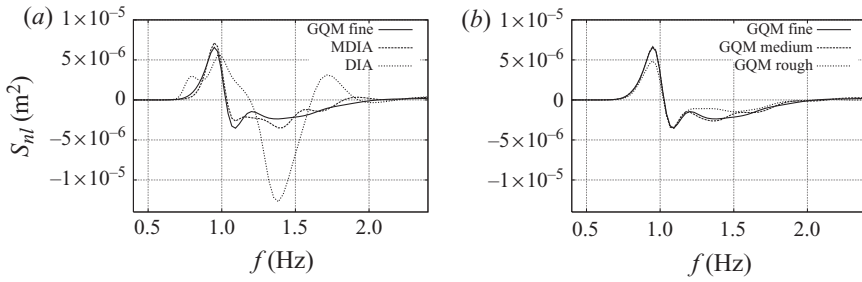


FIGURE 1. Nonlinear transfer term S_{nl} computed with (a) DIA, MDIA and GQM (fine resolution), and (b) GQM (rough, medium and fine resolutions).

MDIA curve gives significantly improved results as compared to the original DIA. At first glance, it may even look more attractive than the GQM-rough curve near the S_{nl} peak. It should be noted that the comparison is made for a particular spectral function (JONSWAP spectrum with a standard set of parameters) and angular averaged S_{nl} terms. The deficiencies of the DIA and MDIA approaches become more pronounced when looking at arbitrary spectral forms and angular distributions. This problem has been detailed by, e.g., Benoit (2005) and Gagnaire-Renou *et al.* (in press). DIA (and MDIA too) can give large deviations for both the S_{nl} term and the resulting spectrum compared to ‘true’ distributions.

The problem related to spectral shapes obtained with approximate methods of calculation of S_{nl} is twofold. First, spectral shapes can differ significantly from ‘true’ ones, which is, evidently, not a good thing if we need accurate information on the spectral or angular structure of the spectrum. The second point seems more critical: distortion of spectral shape affects wave input and dissipation terms that depend on wave spectrum and, hence, corrupts the modelling of essential physics of wind-wave interaction.

There is an important basic property that reconciles both approaches for S_{nl} . The collision integral S_{nl} for deep-water waves obeys the homogeneity property,

$$S_{nl} [\nu N(\nu \mathbf{k})] = \nu^3 \nu^{19/2} S_{nl} [N(\mathbf{k})], \quad (2.9)$$

for arbitrary positive coefficients ν and ν . This basic property should be satisfied both for exact methods (Badulin *et al.* 2005) and for their substitutes like DIA or MDIA irrespective of possible corruption of the resulting spectral shapes. The common property of all the approaches for the collision integral S_{nl} (see (2.9)) raises new non-trivial questions when trying to answer the issue *which approach is more adequate* to research or operational needs. As we shall see below, DIA remains quite good in reflecting essential features of wind-wave growth when looking at integrated parameters (e.g. total wave energy, characteristic frequencies of wave spectrum).

3. Physical scaling of wind-wave growth

Having different models of wind input S_{in} and different approaches for nonlinear transfer term S_{nl} , we are trying to construct a physically transparent coupling scheme of these constituents of wind-wave evolution in a wide range of physical conditions. It calls for an introduction of physical scaling where results for the different conditions could be presented in a comparable form. Here we consider two approaches for such scaling: the traditional wind-speed scaling, associated with the work of Kitaigorodskii (1962), and the so-called weakly turbulent scaling (Badulin *et al.* 2007), closely related

to the phenomenon of cascading due to resonant wave-wave interactions in a random field of weakly nonlinear waves (Zakharov *et al.* 1992).

3.1. Traditional wind-speed scaling

Conventional scaling of wind-wave data often relies on wind speed as a key physical scale (Kitaigorodskii 1962). This scaling introduces non-dimensional fetch, $\chi = xg/U_{10}^2$, and duration, $\tau = tg/U_{10}$, as scales of wind forcing and non-dimensional frequency, $\tilde{\omega} = \omega U_{10}/g$, and energy, $\tilde{E} = Eg^2/U_{10}^4$, as intrinsic characteristics of wave field. (We follow here the ‘oceanographic definition’ of wave energy, $E = m_0 = \langle \eta^2 \rangle$; see (2.4).) Unless otherwise specified, we use 10 m as a reference height for wind speed.

Power-law dependences of non-dimensional total energy \tilde{E} and peak frequency $\tilde{\omega}_p$ on non-dimensional fetch χ ,

$$\tilde{E} = E_0 \chi^{p_\chi}, \quad \tilde{\omega}_p = \omega_0 \chi^{-q_\chi}, \quad (3.1a)$$

or non-dimensional duration τ ,

$$\tilde{E} = E_0 \tau^{p_\tau}, \quad \tilde{\omega}_p = \omega_0 \tau^{-q_\tau}, \quad (3.1b)$$

play an important role in generalization of experimental results.

A good reason for parametrizing wave growth by formulas (3.1) with four free parameters (non-dimensional coefficients ω_0 , E_0 , and exponents $p_{\chi(\tau)}$, $q_{\chi(\tau)}$) could be the universality of these parameters. This is, however, not the case: the scatter of the parameters is too broad (see, for discussion, the introduction of Badulin *et al.* 2007). This also justified the following summary by Donelan *et al.* (1992):

‘Perhaps it is time to abandon the idea that a universal power law for non-dimensional fetch-limited growth rate is anything more than an idealization.’

Wind-speed scaling relies upon ‘an ideal set-up’ of wind-wave growth and explains all outliers by additional physical factors that are absent from this reference ideal case. This approach does not allow for definite indication and quantification of physical mechanisms for these outliers. At the same time, the traditional scaling remains a valuable tool for wind-wave study in so far as it operates with the wind speed, which is an observable parameter.

As stated in §1, Kitaigorodskii (1962) tried to go beyond the formal dimensional analysis. He considered a mechanism of cascading of wave energy in the spirit of the Kolmogorov model of hydrodynamic turbulence. First, the magnitude of the wave spectrum was related to the energy flux in a general form (see (22), (23) in Kitaigorodskii 1962), then the energy flux was parametrized in terms of wind speed ((4) in Kitaigorodskii 1962). Within the same physical analogy, the well-known law ω^{-4} for a spectral range of ‘small-scale isotropic turbulence’ has been proposed (range V of figure 5 in Kitaigorodskii 1962). This consideration anticipated subsequent basic results of the theory of weak turbulence (Zakharov *et al.* 1992).

3.2. The split-balance model and weakly turbulent scaling

The mathematically and physically consistent theory proposed a few years later by Zakharov & Filonenko (1966) and Zakharov (1966) extended the understanding of the wave cascading. It has been found that the wave-spectrum evolution is governed by two types of cascades: the direct one that transfers energy to shorter waves and, then to a dissipation range (Zakharov & Filonenko 1966), and the inverse cascade that provides spectral transfer in the opposite direction (Zakharov & Zaslavsky 1982*b*).

The latter process is considered to be responsible for the well-known phenomenon of downshift of wind-wave spectrum.

Recent studies (Badulin *et al.* 2005, 2007) have shown the leading role of the inverse cascade mechanism and proposed an asymptotic model for the growing wind sea: the so-called split-balance model. This model ‘splits’ effects of nonlinear transfer and external forcing into two equations. In terms of wave action spectral density $N(\mathbf{k})$, it is written as follows:

$$dN_{\mathbf{k}}/dt = S_{nl} [N_{\mathbf{k}}], \quad (3.2a)$$

$$\langle dN_{\mathbf{k}}/dt \rangle = \langle S_{in} + S_{diss} \rangle. \quad (3.2b)$$

Here angle brackets $\langle \cdot \rangle$ mean integration over the whole wavenumber space, $\mathbf{k} = (k_x, k_y)$.

The asymptotic model (3.2) provides families of self-similar solutions for special cases of duration- and fetch-limited growth. These solutions obey the weakly turbulent laws of wind-wave growth (Badulin *et al.* 2007) that links spectral magnitudes with total wave input (spectral flux) $\langle S_{in} + S_{diss} \rangle$. In terms of total energy, one gets (Badulin *et al.* 2007)

$$\frac{E\omega_p^4}{g^2} = \alpha_{ss} \left(\frac{\omega_p^3}{g^2} \langle S_{in} + S_{diss} \rangle \right)^{1/3} = \alpha_{ss} \left(\frac{\omega_p^3}{g^2} \frac{dE}{dt} \right)^{1/3}. \quad (3.3)$$

Here α_{ss} is a parameter of self-similarity that depends slightly on exponents of spatial or temporal growth p_χ , p_τ in (3.1) (Badulin *et al.* 2007):

$$\alpha_{ss}^{(f)} \sim p_\chi^{-1/3}, \quad \alpha_{ss}^{(d)} \sim p_\tau^{-1/3}. \quad (3.4)$$

Below we omit superscripts (d) and (f) for duration- and fetch-limited cases. Note that the exponents 1/3 in (3.3) and (3.4) come from the cubic nonlinearity of the Hasselmann equation (1.1): wave energy is proportional to energy flux to the power one-third, in contrast to Kitaigorodskii’s analogy with the Kolmogorov turbulence, where energy is a linear function of energy flux (see (30) in Kitaigorodskii 1962).

The model (3.2) and the weakly turbulent law (3.3) operate with integral net input $\langle S_{in} + S_{diss} \rangle$. Thus, the model postulates independence of wave evolution from details of wind-wave coupling. This robustness of the model (3.2) and quantitative link (3.3) makes the corresponding weakly turbulent scaling a really powerful tool of wind-wave studies.

Self-similarity relationship (3.3) can also be introduced in different forms for wave momentum M ,

$$\frac{M\omega_p^3}{g^2} = \alpha_{ss}^{(M)} \left(\frac{\omega_p^2}{g^2} \frac{dM}{dt} \right)^{1/3}, \quad (3.5)$$

or wave action N ,

$$\frac{N\omega_p^5}{g^2} = \alpha_{ss}^{(N)} \left(\frac{\omega_p^4}{g^2} \frac{dN}{dt} \right)^{1/3}, \quad (3.6)$$

where the self-similarity parameters $\alpha_{ss}^{(M)}$, $\alpha_{ss}^{(N)}$ are counterparts of α_{ss} in (3.3). Thus, one can use the weakly turbulent scaling for different physical values, which extends our understanding of wave dynamics and wind-wave coupling itself.

We should stress once more a conceptual difference between weakly turbulent scaling and traditional wind-speed scaling. The latter links wind characteristics directly

with wave parameters. Additionally, it relies (somewhat implicitly) upon an idea of universality of wind speed as a characteristic of air flow that governs wave evolution. In fact, discrepancies of experimental results themselves in the form of dependences (3.1) with four free parameters (ω_0 , E_0 , $p_{\chi(\tau)}$, $q_{\chi(\tau)}$) contradict this idea of universality. On the contrary, the weakly turbulent scaling separates the air-flow dynamics from inherent wave dynamics assuming the dominating role of nonlinear transfers. This hypothesis makes the total wave forcing a key physical parameter and gives a quantitative link between total wave forcing and integral parameters of wave spectrum. Parameters ω_0 , E_0 , $p_{\chi(\tau)}$, $q_{\chi(\tau)}$ in (3.1) cease to be free but obey two relationships resulting from the split-balance model (see (2.10), (2.21), (2.38), (2.41) in Badulin *et al.* 2007). These self-similarity relationships have been used by Badulin *et al.* (2007, 2008a) for validating the asymptotic split-balance model (3.2) and for numerical estimates of self-similarity parameter α_{ss} for the case of duration-limited growth.

For the fetch-limited growth, the law (3.3) in the form

$$\frac{E\omega_p^4}{g^2} = \alpha_{ss} \left(\frac{\omega_p^2}{2g} \frac{\partial E}{\partial x} \right)^{1/3} \quad (3.7)$$

has been checked by Badulin *et al.* (2007) for a collection of experimental power-law parametrizations of wind-wave growth covering a wide range of energy growth exponents,

$$0.7 < p_{\chi} < 1.1. \quad (3.8)$$

After thorough selection of the cleanest experiments (the best fit to the idealization of the fetch-limited growth), the self-similarity parameter α_{ss} has been estimated as (Badulin *et al.* 2007)

$$\alpha_{ss} = 0.55 \pm 0.25. \quad (3.9)$$

Analysing results of the present simulations, we are trying to use advantages of weakly turbulent scaling in the sense of laws (3.3), (3.5), (3.6) and give a numerical justification of (3.7) for the fetch-limited wave growth.

3.3. Reference cases of wind-wave growth

Weakly turbulent laws of wind-wave growth of the form (3.3), (3.5), (3.6) make it possible to fix reference cases corresponding to different regimes of wave dynamics at different stages of wave growth. These cases correspond to constant fluxes of energy, wave momentum or wave action, and give simple single-parameter dependences of energy on peak frequency. The theoretical and experimental aspects will be presented in detail in a separate paper. Here we discuss these reference cases in brief as a background for analysis of our simulation results. All these cases have been known for a long time but their relevance to weak turbulence theory had not yet been considered.

3.3.1. The Toba 3/2 law as a regime of constant energy flux to waves

The relevance of Toba's empirical 3/2 law as a basic regime of wave growth was shown by Badulin *et al.* (2007). Take Toba's law for significant wave height H_s and period T_s (Toba 1972),

$$H_s = B(gu_*)^{1/2} T_s^{3/2}. \quad (3.10)$$

Conversion to total energy $E = H_s^2/16$ and peak frequency $\omega_p \approx 2\pi/T_s$ gives

$$\frac{E\omega_p^4}{g^2} = \left(\frac{\pi^9 B^6 u_*^3 \omega_p^3}{8g} \frac{\omega_p^3}{g^2} \right)^{1/3}. \quad (3.11)$$

Comparing (3.11) and (3.3), we see that Toba's law corresponds to constant in time total flux of energy dE/dt . This flux, or total net input, can be easily estimated by (note the misprint in (5.1) of Badulin *et al.* 2007)

$$\frac{dE}{dt} = \frac{\pi^9 B^6 u_*^3}{8\alpha_{ss}^3 g} = 0.16 \frac{\rho_a}{\rho_w} \frac{u_*^3}{\alpha_{ss}^3 g}, \quad (3.12)$$

when $B = 0.062$ (Toba 1972). The estimate of wave energy looks reasonable. In terms of explicit dependence on fetch, this case gives exponents $p_\chi = 3/4$, $q_\chi = 1/4$ in (3.1). The growth is lower than a linear one because of the downshift effect: longer waves at longer fetches travel faster.

3.3.2. The Hasselmann *et al.* (1976) 5/3 law of constant momentum flux to waves

Hasselmann *et al.* (1976) considered a special case that gives a single-parameter 5/3 law linking significant wave height and peak period. In terms of non-dimensional energy, we can write

$$\tilde{E} = C_0 \left(\frac{\tilde{\omega}_p}{2\pi} \right)^{-10/3}, \quad C_0 = 5.1 \times 10^{-6}. \quad (3.13)$$

The term 'law' seems to be quite relevant: this case corresponds to constant flux of momentum to waves, i.e. $dM/dt = \text{constant}$ in (3.5). It is interesting to recall attempts by Toba (1978) to identify this case with his own law when experimental data are close to both 3/2 (see (3.10)) and 5/3 (see (3.13)) dependences. From the 'weakly turbulent viewpoint', the difference between these two laws is fundamental: Toba's 3/2 law applies for constant energy flux while the 5/3 law is valid for constant flux of wave momentum. From (3.3), one immediately has the following estimate of energy growth rate:

$$\frac{dE}{dt} = 7.7 \times 10^{-3} \frac{\rho_a}{\rho_w} \frac{C_p u_*^2}{\alpha_{ss}^3 g}. \quad (3.14)$$

Here we used dependence of reference wind speed U_{10} and friction velocity u_* in the simplest form,

$$U_{10} = 28u_*. \quad (3.15)$$

For a growing wind sea, the spectral peak phase speed C_p is growing and, hence, the energy production is growing as well. In terms of explicit dependence on fetch, it gives a linear growth of energy ($p_\chi = 1$). The frequency downshift ($q_\chi = 3/10$) is faster than in the previous Toba case.

3.3.3. The Zakharov & Zaslavsky (1983b) 4/3 law of constant action flux to waves

The last reference case of wave growth has been found by Zakharov & Zaslavsky (1983b, see also thesis by Zaslavsky, 1984 for details). In a series of papers, Zakharov & Zaslavsky (1982a,b, 1983a,b) first applied the weakly turbulent theory for analysing wind-driven seas where wave growth has been associated with inverse cascading of wave action. They started with the classic stationary solution describing constant flux of wave action from infinitely small to infinitely large wave scales (Zakharov & Zaslavsky 1982a). Extending this mechanism to the non-stationary case, they proposed

an explanation of experimental data available in the early 1980s. The theory gave exponents of energy growth and frequency downshift in (3.1) while experimental data were used to find the corresponding pre-exponents. The energy-to-frequency relationship was found from JONSWAP data (Hasselmann, Dunkel & Ewing 1980),

$$\tilde{E} = 1.5 \times 10^{-3} \tilde{\omega}_p^{-8/3}, \quad (3.16)$$

for theoretical exponents,

$$p_\chi = 4/7, \quad q_\chi = 3/14. \quad (3.17)$$

As in previous cases and with (3.15), one has for energy input

$$\frac{dE}{dt} = 1.6 \frac{\rho_a}{\rho_w} \frac{C_p^{-1} u_*^4}{\alpha_{ss}^3 g}. \quad (3.18)$$

The energy input (3.18) (for a constant friction velocity u_*) decreases with time as the peak frequency ω_p .

3.4. Wave growth as a consequence of different regimes of wind-wave coupling

The three reference cases presented above allow us to construct a physically consistent scheme of wave growth as a series of regimes of wind-wave coupling.

Relatively young waves obey the 5/3 law by Hasselmann *et al.* (1976). This growth is controlled by permanent wind stress as long as wave momentum flux is constant. The energy growth rate of these waves increases with time.

The famous 3/2 law by Toba (1972) corresponds to constant wave energy flux while wave momentum flux decays. In other words, the contribution of wind stress to wave production decays at this stage of wave growth. Toba himself treats this law within his heuristic theory as a sort of ‘saturation’ of wave growth (Toba 1997). Within our approach, it is seen as a regime of maximal wave energy production. Older waves evolve in accordance with the 4/3 law by Zakharov & Zaslavsky (1983*b*), i.e. wave energy flux decays. Thus, following Toba, one can treat the 5/3 regime as ‘under-saturated’ when energy input is growing with the wave growth, while the 4/3 case, logically, can be called ‘over-saturated’ when energy input is decaying.

We conclude this section by presenting two tables. Table 1 presents the three reference cases (the 5/3, 3/2 and 4/3 laws), the corresponding exponents and estimates of wave energy inputs. Table 2 gives exponents T , p_χ , q_χ as well as pre-exponents \tilde{B} for three ‘cleanest’ wave growth dependences, as selected by Badulin *et al.* (2007) (see their tables 2 and 3). When experimental exponents p_χ , q_χ do not precisely obey the relationship predicted by the weakly turbulent theory, we also give a theoretical value of exponent $T_{th} = 5p_\chi / (2p_\chi + 1)$ (see (2.38) of Badulin *et al.* 2007), considering the exponent of wave energy growth with fetch as ‘more reliable’ than the exponent of frequency downshift q_χ . All the experimental dependences are well between the Toba (1972) 3/2 and the Hasselmann *et al.* (1976) 5/3 laws. Within the weakly turbulent approach presented above, it means energy flux growing slowly with fetch. Estimates of the corresponding rates of wave energy input can be derived from wave growth law (3.3) in the same way as for reference cases of table 1.

The theoretical cases of table 1 and experimental dependences of table 2 are used below for analysis of numerical results on wind-wave growth. Within this analysis, firstly, we discuss the evolution of key parameters of wave spectrum: total energy and peak frequency. Secondly, theoretical estimates of net wave forcing can be compared to S_{in} and S_{diss} given by models of wind input and dissipation. Thus, one can try to discriminate between features of inherent wave physics and physics of wind-wave coupling.

| Case | $T = p_\chi/(2q_\chi)$ | \tilde{B} | p_χ | q_χ | $\rho_w/\rho_a \times dE/dt$ |
|--|------------------------|-----------------------|----------|----------|--|
| $dM/dt = \text{constant}$ (Hasselmann <i>et al.</i> 1976) | 5/3 | 2.33×10^{-3} | 1 | 3/10 | $0.0077 \frac{C_p u_z^2}{\alpha_{ss}^3 g}$ |
| $dE/dt = \text{constant}$ (Toba 1972) | 3/2 | 2.13×10^{-3} | 3/4 | 1/4 | $0.16 \frac{u_z^2}{\alpha_{ss}^3 g}$ |
| $dN/dt = \text{constant}$ (Zakharov & Zaslavsky 1983b) | 4/3 | 1.5×10^{-3} | 4/7 | 3/14 | $1.6 \frac{C_p^{-1} u^4}{\alpha_{ss}^3 g}$ |

TABLE 1. Summary of reference regimes of wind-wave growth. Exponents p_χ , q_χ are given for explicit dependences on fetch (3.1). \tilde{B} and T are parameters in energy-to-frequency relationship $\tilde{E} = \tilde{B} \tilde{\omega}_p^{-2T}$. The last column is parametrization of net wave forcing dE/dt in accordance with weakly turbulent relationship (3.3).

| Case | $T = \frac{p_\chi}{2q_\chi}$ | \tilde{B} | p_χ | q_χ | $T_{th} = \frac{5p_\chi}{2p_\chi+1}$ |
|---------------------------------|------------------------------|-----------------------|----------|----------|--------------------------------------|
| Babanin & Soloviev (1998a) | 1.62 | 2.91×10^{-3} | 0.89 | 0.275 | 1.60 |
| Kahma & Calkoen (1992) unstable | 1.68 | 3.99×10^{-3} | 0.94 | 0.28 | 1.63 |
| Kahma & Calkoen (1992) stable | 1.58 | 2.43×10^{-3} | 0.76 | 0.24 | 1.51 |

TABLE 2. Summary of experimental cases of wind-wave growth. Exponents p_χ , q_χ are given for explicit dependences on fetch (3.1). \tilde{B} and T are parameters in the corresponding energy-to-frequency relationship $\tilde{E} = \tilde{B} \tilde{\omega}_p^{-2T}$. The last column is the theoretical estimate of exponent T in the energy-to-frequency relationship (Badulin *et al.* 2007) for the given value of p_χ .

4. Scaling of fetch-limited wind-wave growth

In this section, we discuss results of fetch-limited numerical simulations within different physical approaches. First, we use the traditional wind-speed scaling, and then we try to extend our analysis by applying a weakly turbulent approach.

4.1. Wind-speed scaling of fetch-limited growth

4.1.1. Explicit dependences of energy and frequency on fetch

The simulation results can be presented straightforwardly in terms of conventional non-dimensional variables (Kitaigorodskii 1962, 1983): non-dimensional energy $\tilde{E} = Eg^2/U_{10}^4$ and spectral peak frequency $\tilde{\omega}_p = U_{10}/C_p$ (inverse wave age) as functions of non-dimensional fetch $\chi = xg/U_{10}^2$. In figures 2 and 3, results for each value of wind speed are presented in separate panels for two different wind input functions S_{in} and two different methods for calculating S_{nl} . Straight lines show the experimental ‘cleanest’ dependences of table 2. One can see a strong dispersion in both numerical and experimental dependences. While experimental curves are fixed in all panels, their numerical counterparts drift with wind speed within almost one order of magnitude for non-dimensional energy (figure 2) and by several tens of percentage points for non-dimensional frequency (figure 3). In all the panels of figures 2 and 3, we see, first of all, differences dealing with wave input functions. The non-dimensional energy \tilde{E} obtained by Janssen (1989, 1991) reaches magnitudes twice as high as that obtained with the input of Snyder *et al.* (1981). The corresponding difference for $\tilde{\omega}_p$ can reach 20%. The effect of method of calculation of nonlinear

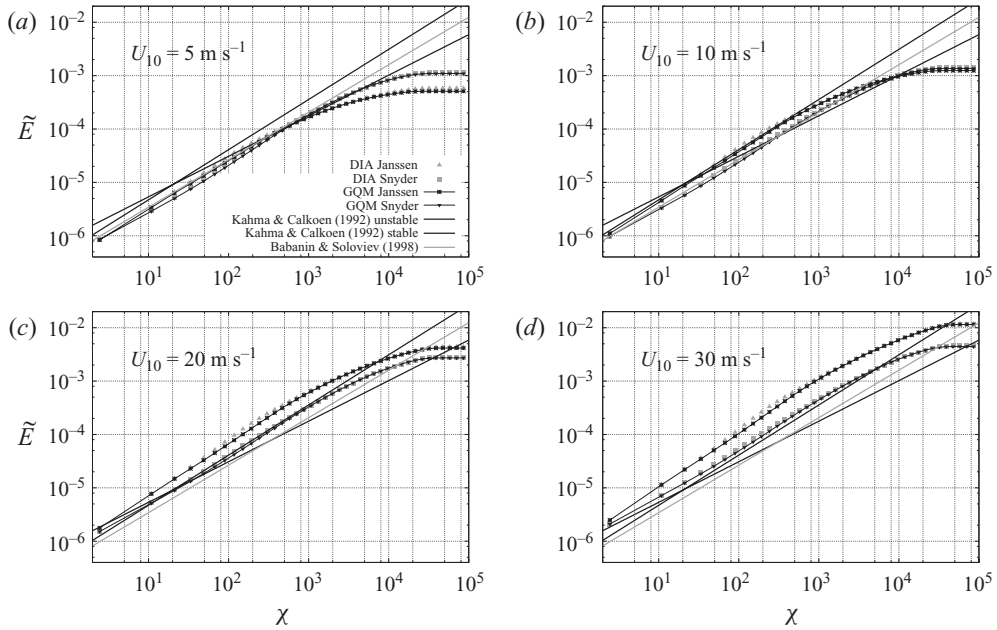


FIGURE 2. Non-dimensional energy $\tilde{E} = Eg^2/U_{10}^4$ as a function of non-dimensional fetch $\chi = xg/U_{10}^2$, for different wind speeds $U_{10} = 5, 10, 20, 30 \text{ m s}^{-1}$, parametrizations of wave input term S_{in} by Snyder *et al.* (1981) and Janssen (1989, 1991), DIA and GQM for calculating S_{nl} (shown in legends). ‘The cleanest’ experimental dependences of table 2 are given for comparison.

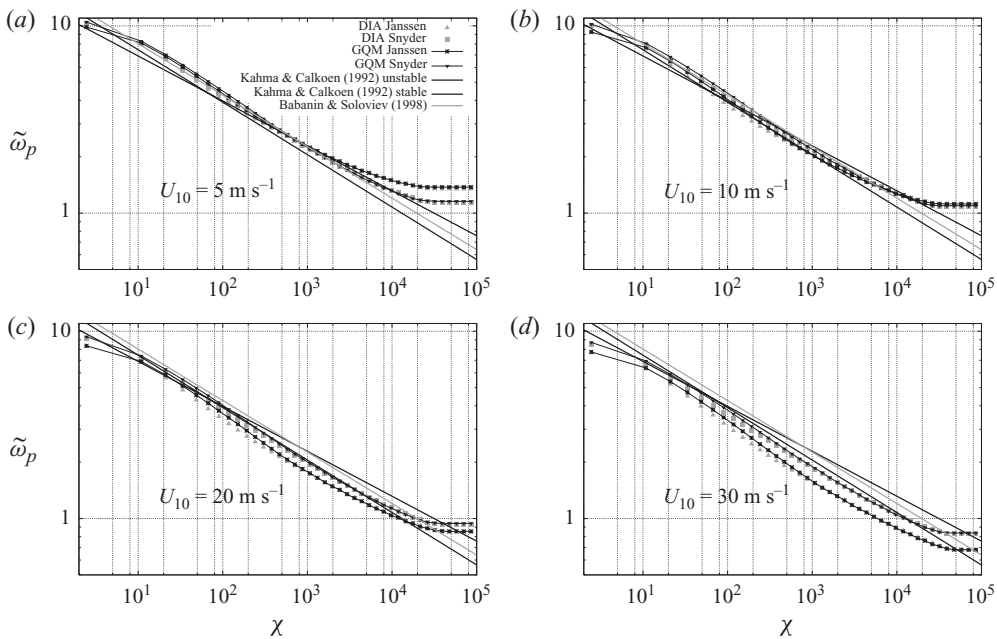


FIGURE 3. Inverse wave age $\tilde{\omega}_p = \omega_p U_{10}/g$ as a function of non-dimensional fetch $\chi = xg/U_{10}^2$, for different wind speeds, $U_{10} = 5, 10, 20, 30 \text{ m s}^{-1}$, parametrizations of wave input term S_{in} by Snyder *et al.* (1981) and Janssen (1989, 1991), DIA and GQM for calculating S_{nl} (see legends). ‘The cleanest’ experimental dependences of table 2 are given for comparison.

transfer term S_{nl} is incomparably weaker but is still visible for relatively young waves.

Effect of wind speed on growth curves is also clearly seen in figures 2 and 3: for low winds ($U_{10} = 5 \text{ m s}^{-1}$), waves grow faster when using input by Snyder *et al.* (1981), while for high winds ($U_{10} = 20\text{--}30 \text{ m s}^{-1}$), the input by Janssen (1989, 1991) leads to stronger growth. As compared with dependences of table 2, both input functions can give lower (at low winds, $U_{10} = 5, 10 \text{ m s}^{-1}$) or faster (at strong winds, $U_{10} = 20, 30 \text{ m s}^{-1}$) initial evolution.

Within this conventional scaling, only two qualitatively different stages of wave development can be identified: growing wind sea and mature sea. When whitecapping dissipation grows with fetch faster than wave input, energy and peak frequency can cease to evolve. In fact, the very existence of mature sea where all the terms on the right-hand side of (1.1) are fully balanced is an open question that is far from being resolved (Komen *et al.* 1984). Further, in this paper, we refer to the mature sea state only in terms of total energy and spectral peak frequency. A separation line between growing and mature sea can be drawn in an arbitrary way in quite a wide range of non-dimensional fetches (20 000–40 000 in our simulations). Moreover, the state of ‘mature’ sea does not appear to be universal in terms of non-dimensional wave energy and frequency. This contradicts the classic Pierson & Moskowitz (1964) parametrization of wave spectrum where universal values of wave age and wave steepness are postulated.

Thus, the analysis of wave evolution within the traditional wind-speed scaling leads to trivial conclusions like the following one: the energy is higher when total input is higher. It allows us to qualitatively (not quantitatively) explain different energies of growing waves and different magnitudes of the mature seas at long fetches. At the same time, a remarkable correlation should be noted between energy and peak frequency curves: higher magnitudes of the mature sea amplitudes correspond to lower spectral peak frequencies (cf. figures 2 and 3).

Friction velocity u_* is usually regarded as a more physically based scale in comparison with wind speed at a reference height, say, U_{10} . Our analysis shows that the friction velocity scaling essentially reduces dispersion of curves for different wind speeds with the same input function. However, dispersion between the curves obtained with different wind input functions is still very pronounced, sometimes even more pronounced than with scaling by U_{10} . Skipping details of this comparison, we can conclude here that friction velocity (as well as other speed scales) does not appear as a universal scale of wave evolution (in terms of non-dimensional energy \tilde{E} and frequency $\tilde{\omega}_p$).

4.1.2. *The single-parameter dependences*

The single-parameter representation of energy \tilde{E} versus peak frequency $\tilde{\omega}_p$ has been discussed in our overview of reference cases in §3.3. An advantage of this approach is an absence of explicit dependence on fetch, and, hence, probably, a less pronounced dependence on features of wave forcing.

In figure 4, dependences of non-dimensional energy on non-dimensional peak frequency are given similarly to figures 2 and 3 for different wind speeds, parametrizations of wave forcing terms and methods of calculation for S_{nl} . Dispersion of all the results looks unessential. Moreover, the mature sea state (upper left simulation points) and growing seas are difficult to distinguish in these plots because of fast convergence of total energy and peak frequency to limiting values.

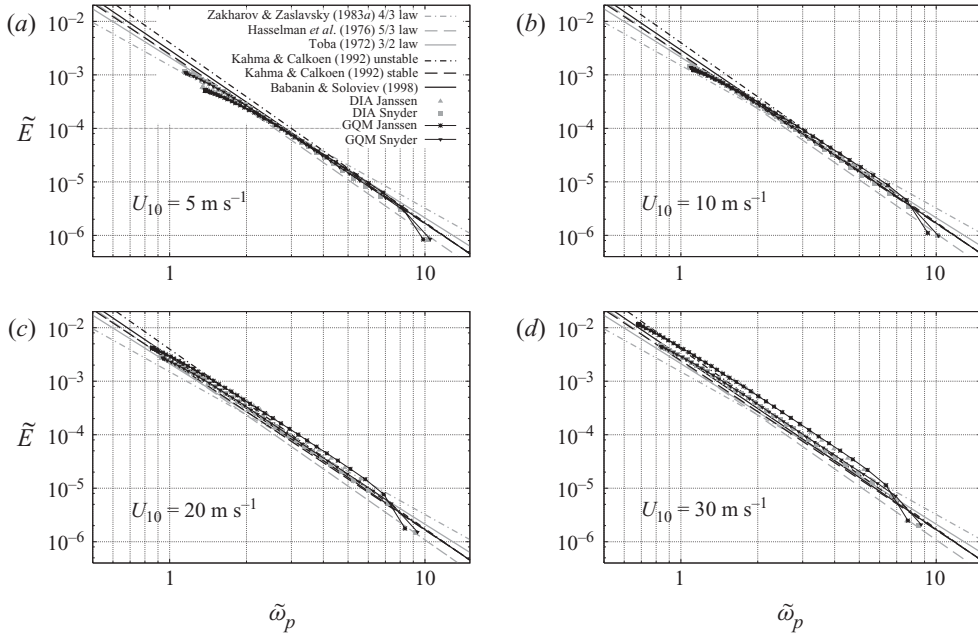


FIGURE 4. Non-dimensional energy \tilde{E} versus non-dimensional peak frequency $\tilde{\omega}_p$. Black lines, ‘the cleanest’ experimental dependences; grey lines, Toba’s 3/2 law for the reference case $dE/dt = \text{constant}$, the Hasselmann *et al.* (1976) 5/3 law for the case $\omega_p dE/dt = \text{constant}$ and the Zakharov & Zaslavsky (1983b) 4/3 law for the case $\omega_p^{-1} dE/dt = \text{constant}$; symbols, numerical simulations.

All the dependences listed in tables 1 and 2 give very close fit (at first glance) to the results of simulations. These minor mismatches, in fact, are of key importance from the weakly turbulent viewpoint: small deviation in energy being converted into energy flux becomes significant when $dE/dt \sim E^3$ (see (3.3)). Thus, the mismatches, being uninformative in terms of single-parametric dependences, indicate a significant difference in net wave input (total wave forcing $\langle S_{in} + S_{diss} \rangle$), a key parameter of weakly turbulent scaling. With careful inspection, one can notice that the slopes of the simulation curves are close to Hasselmann *et al.* (1976) law for relatively young waves, and later they appear closer to the curve of Toba (1972) and finally to the Zakharov & Zaslavsky (1983b) plot at the end of the growing wind sea stage.

4.2. Flux scaling of fetch-limited growth

The weakly turbulent scaling is based on total wave inputs (fluxes) of basic quantities: wave energy, wave momentum, wave action. In this paper, we use energy flux only. For self-similar solutions, the energy flux can be converted easily to fluxes of wave momentum or wave action and, thus, results can be related easily to reference cases considered in the previous section.

4.2.1. Total wave input as physical scale

The role of total wave input as a key physical scale cannot be adequately understood separately from the split-balance model presented in § 3.2 and the resulting energy-to-flux relationship (3.3). Nevertheless, we start with trivial analysis of dimensional net wave input in order to show effects of wave input parametrization on wave evolution.

Figure 5 shows net wave input $\langle S_{in} + S_{diss} \rangle$ for high winds and the resulting wave heights and periods as functions of dimensional fetch for different wave input parametrizations and the DIA method for nonlinear transfer terms. With S_{in} parametrization by Janssen (1989, 1991), the total wave forcing $\langle S_{in} + S_{diss} \rangle$ appears to be two to three times higher than the one by Snyder *et al.* (1981) for the same wind speed $U_{10} = 30 \text{ m s}^{-1}$. The Janssen (1989, 1991) function at $U_{10} = 26 \text{ m s}^{-1}$ is shown as one that is close to the Snyder *et al.* (1981) input at $U_{10} = 30 \text{ m s}^{-1}$. Figure 5 reflects a trivial fact: when the net input is higher, the wave amplitudes are higher. Additionally, reference net wave inputs (wave energy fluxes) of table 1 are plotted for comparison. They appear almost one order of magnitude below functions obtained in simulations. This significant difference can be related to high wind speeds that have been rarely observed in the experiments on which the reference cases are based (Toba, Hasselmann *et al.*, JONSWAP data). Strictly speaking, high winds are not covered either by the Snyder experimental parametrization used in our simulations, which was also justified for weak winds. At the same time, there is a qualitative correspondence of reference cases and results of simulations: wave input grows at short fetches (the 5/3 law of Hasselmann *et al.* 1976), reaches a stationary state for intermediate fetches (the 3/2 regime of Toba 1972) and then decays as predicted by Zakharov & Zaslavsky (1983*b*). Note that for the reference cases, we used net wave input parametrizations of table 1 with $\alpha_{ss}(p_\chi = 1) = 0.62$ (Hasselmann *et al.* 1976), $\alpha_{ss}(p_\chi = 3/4) = 0.68$ (Toba 1972) and $\alpha_{ss}(p_\chi = 4/7) = 0.74$ (Zakharov & Zaslavsky 1983*b*). The corresponding estimates are based on results of simulations and are detailed below.

Two important points should be stressed. Firstly, rather good quantitative correspondence of H_{m0} , T_p can be reached by simple tuning of total wave input: curves for wind speeds $U_{10} = 26 \text{ m s}^{-1}$ with input by Janssen and $U_{10} = 30 \text{ m s}^{-1}$ with one by Snyder *et al.* (1981) are quite close when total quantities of wave input are close to each other (see figure 5*a* at $500 < x < 3000 \text{ km}$). Secondly, waves very quickly ‘forget’ their previous history: the coincidence of trajectories in figure 5(*b, c*) occurs with rather short delay after coincidence of the curves for total wave input.

Figure 6 shows dependences of net energy input, wave height and period on fetch for low wind, $U_{10} = 10 \text{ m s}^{-1}$, different input functions S_{in} and methods for S_{nl} . The difference between net wave inputs is not so pronounced as in previous case. Additionally, the inputs’ magnitudes appear to be closer to reference cases of table 1 (two to three times versus almost one order for $U_{10} = 30 \text{ m s}^{-1}$). Close wave inputs at large fetches lead, evidently, to close curves for H_{m0} , T_p .

The effect of the method for computing S_{nl} on total wave input is illustrated by figure 6. For short and long fetches (less than 2 km and more than 100 km, respectively), DIA enhances total wave input (up to 50 % for Janssen’s formulation). At short fetches, it leads to a visible effect on wave height H_{m0} and T_p . The mechanism of influence of the method for calculating S_{nl} on wave input and, thus, on the resulting wave growth is illustrated by figure 7. Wave input and dissipation functions depend on spectral distributions since they are quasi-linear in spectral densities. These distributions can differ significantly for the DIA and GQM approaches as is seen in figure 7(*a*). The effect is not easy to assess in so far as nonlinear transfer and external forcing appear to be closely linked. Figure 7 shows the effect of spectral shape on wave input and dissipation for instantaneous spectra at dimensional fetch $x = 2400 \text{ km}$ and $U_{10} = 30 \text{ m s}^{-1}$, i.e. for the mature sea state where the total energy and peak frequency for GQM and DIA are identical. Input functions of Snyder *et al.* (1981)

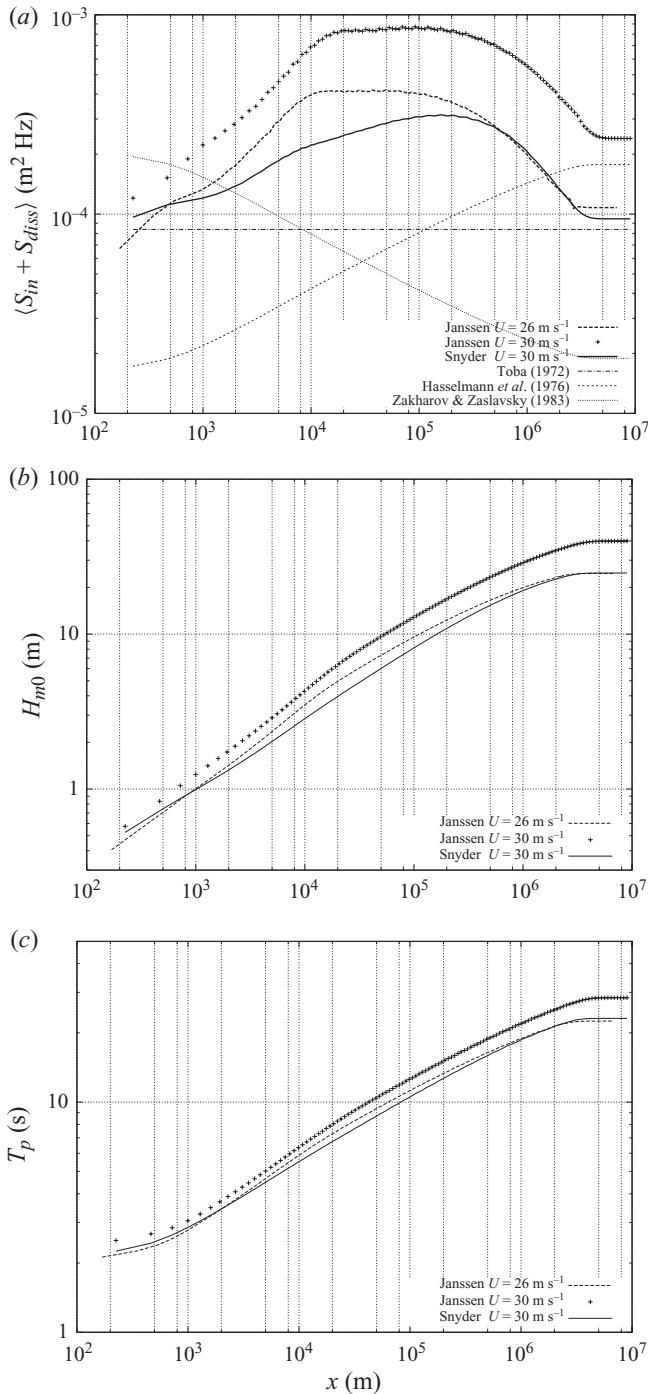


FIGURE 5. (a) Net wave forcing $\langle S_m + S_{diss} \rangle$ as a function of the dimensional fetch x and reference cases of table 1; (b) wave height; and (c) wave period. Snyder's input term S_m at wind speed $U_{10} = 30 \text{ m s}^{-1}$ is compared with Janssen's input term at $U_{10} = 26 \text{ m s}^{-1}$ and $U_{10} = 30 \text{ m s}^{-1}$. Results for DIA for the S_{nl} term are shown.

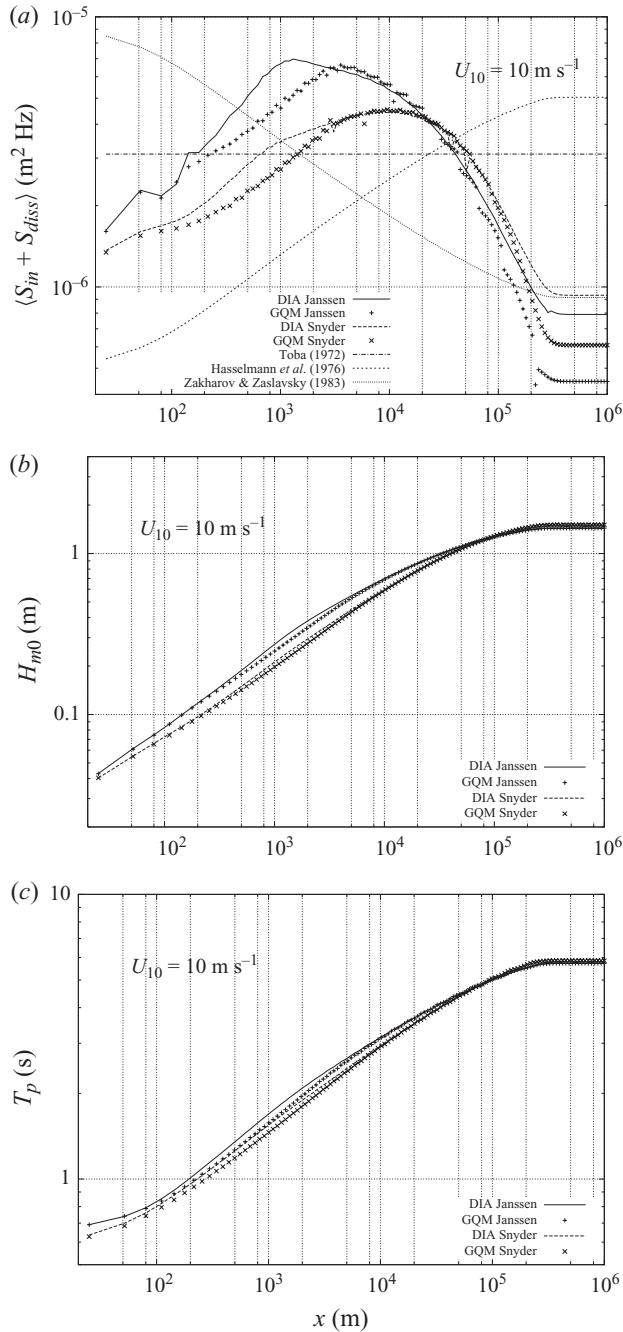


FIGURE 6. (a) Net wave forcing $\langle S_{in} + S_{diss} \rangle$ as a function of the dimensional fetch x and reference cases of table 1; (b) wave height; (c) wave period at wind speed $U_{10} = 10 \text{ m s}^{-1}$ for Snyder and Janssen parametrizations of S_{in} . Results for DIA and GQM are shown.

and Janssen (1989, 1991) and dissipation of Komen *et al.* (1984) are applied to these two spectra. The effect of the spectral shape on the S_{in} and S_{diss} functions is quite easily seen (figure 7b).

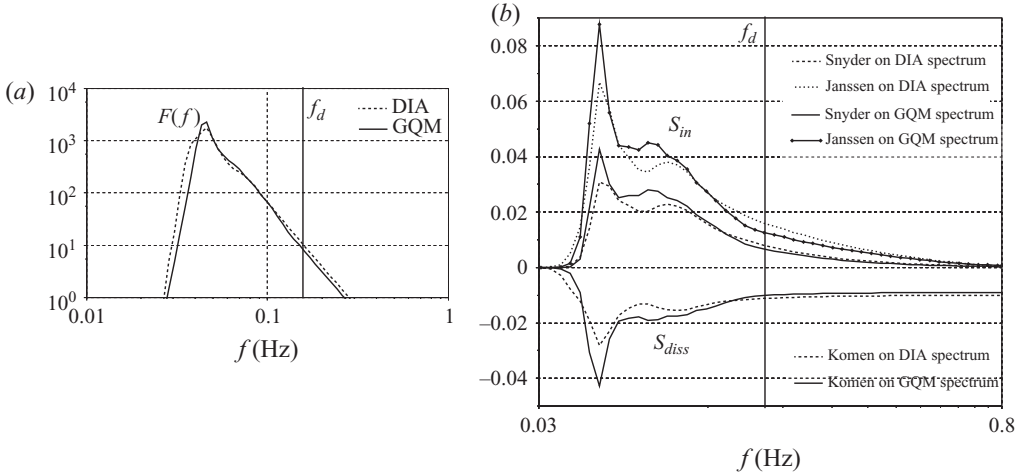


FIGURE 7. (a) One-dimensional spectra $F(f)$ ($\text{m}^2 \text{Hz}^{-1}$) as functions of frequency f (Hz) at a large fetch (2400 km) calculated with GQM and DIA, Snyder's source term and wind speed $U_{10} = 30 \text{ m s}^{-1}$; (b) S_{in} functions of Snyder *et al.* (1981) and Janssen (1989, 1991) and S_{diss} function of Komen *et al.* (1984) applied for these two spectra.

The black vertical line in figure 7 shows the frequency above which the diagnostic tail is imposed in the simulation. To the right of this line, the obtained S_{in} and S_{diss} functions have no influence on the evolution of the spectrum and must not be considered in the calculation of the total wave forcing. Nevertheless, it is interesting to note the strong dissipation in the high-frequency range obtained with the Komen *et al.* (1984) S_{diss} function when imposing a f^{-4} high-frequency tail (see Banner & Young 1994 and Gagnaire-Renou *et al.* 2010 for a discussion of the influence of the constrained tail).

Despite these 'shape-to-input' effects, we see that differences between DIA and GQM growth curves are still very small in figures 2 and 3. This implies that shape-to-input effects are likely in counterbalance with direct effects of the method for calculating S_{nl} .

4.2.2. Method of energy-flux diagrams and self-similarity of wave growth

In this section, we present a method of analysis of wind-wave growth proposed by Badulin *et al.* (2007) and called energy-flux diagrams. The idea of the method is quite simple: the wave evolution is represented by one-parametric dependence of a non-dimensional energy on a non-dimensional characteristic of energy flux.

In a sense, this representation is similar to energy-frequency dependences within the traditional wind-speed scaling considered in §4.1.2, in so far as in both cases we formally follow a dimensional analysis of a physical problem. At the same time, our energy-flux analysis is conceptually different from traditional wind-speed scaling as it is based on an asymptotic physical model (3.2). Accepting this model, we also accept the corresponding scaling. This is in contrast to wind-speed scaling which, currently, cannot be associated with a model of wind-wave coupling in a wide range of physical conditions.

Following Badulin *et al.* (2005, 2007), which showed validity of the asymptotic split-balance model in a wide range of physical conditions, let us introduce two

non-dimensional parameters for further analysis. Wave steepness squared,

$$\varepsilon^2 = \frac{E\omega_p^4}{g^2}, \quad (4.1)$$

replaces non-dimensional energy \tilde{E} of traditional scaling. Note that ε depends only on instantaneous wave characteristics and does not explicitly depend on external forcing (say, on wind speed). The second non-dimensional parameter is dictated by total wave input as a key parameter of external forcing in the split-balance model (3.2):

$$\psi = \frac{\omega_p^3 dE/dt}{g^2}. \quad (4.2)$$

For the fetch-limited case, this value has been written as follows (Badulin *et al.* 2007):

$$\psi = \frac{\omega_p^2 \partial E / \partial x}{2g}. \quad (4.3)$$

Presenting simulation results of the full kinetic equation (1.1) in terms of these two non-dimensional parameters, ε^2 and ψ , we presuppose validity of our asymptotic model in a certain physical range and our ability to physically interpret the deviations from the model beyond this range. The split-balance model relies upon instantaneous integral parameters of wave spectrum and wave input. The full kinetic equation (1.1) is much richer and potentially describes more ‘details’ of wind-wave coupling. One of the goals of the following analysis is to fix the presence of these details and, in some cases, to identify their physical nature.

The energy-flux diagram corresponding to our numerical simulations of fetch-limited growth is presented in figure 8. All cases (different wind speeds, models of S_{in} , methods for S_{nl}) are intentionally plotted in this figure. One can see an asymptotic stage of weakly turbulent wave development fairly well as a linear dependence of wave steepness squared, ε^2 , on non-dimensional total wave input ψ in power 1/3. This is in perfect agreement with the asymptotic relationship (3.7). The three experimental dependences of table 2 are given for comparison. Deviations from the asymptotic regime are seen as different stages of wind-sea evolution. These different stages (initial wave growth, growing wind sea and mature wind sea) are described consecutively below.

The self-similarity parameter α_{ss} controls the ratio of instantaneous wave steepness squared, ε^2 , to non-dimensional net wave input parameter, $\psi^{1/3}$. Results of our numerical study show that straight line $\varepsilon^2 = \alpha_{ss} \psi^{1/3}$ with $\alpha_{ss} = 0.68$ (light blue curve in figure 8) is tangent to a bundle of curves and consequently $\alpha_{ss} = 0.68$ can be taken as a representative estimate of the self-similarity parameter. In fact, parameter α_{ss} depends on wave growth rate p_χ (see (3.4)). Trying to determine a confidence interval for α_{ss} , we fix the Toba case as reference one, representative for many of the observations: $\alpha_{ss}(p_\chi = 3/4) = 0.68$. Then a value of α_{ss} for the two other reference cases of table 1 can be easily deduced from approximate proportionality, $\alpha_{ss} \sim p_\chi^{-1/3}$ (see (3.4)): $\alpha_{ss}(p_\chi = 1) = 0.62$ (Hasselmann *et al.* 1976) and $\alpha_{ss}(p_\chi = 4/7) = 0.74$ (Zakharov & Zaslavsky 1983b). Estimates of α_{ss} for reference cases of Hasselmann *et al.* (1976) and Zakharov & Zaslavsky (1983b) differ from the Toba value by less than 10 %. The two bounds of the self-similar development stage can, thus, be defined as $\alpha_{ss} = 0.68 \pm 0.1$, which gives less than 15 % error, consistent with estimates of reference cases. The estimate $\alpha_{ss} = 0.68 \pm 0.1$ is represented in figure 9 where lines $\alpha_{ss} = 0.58$, $\alpha_{ss} = 0.68$ and $\alpha_{ss} = 0.78$ are plotted for a better visualization.

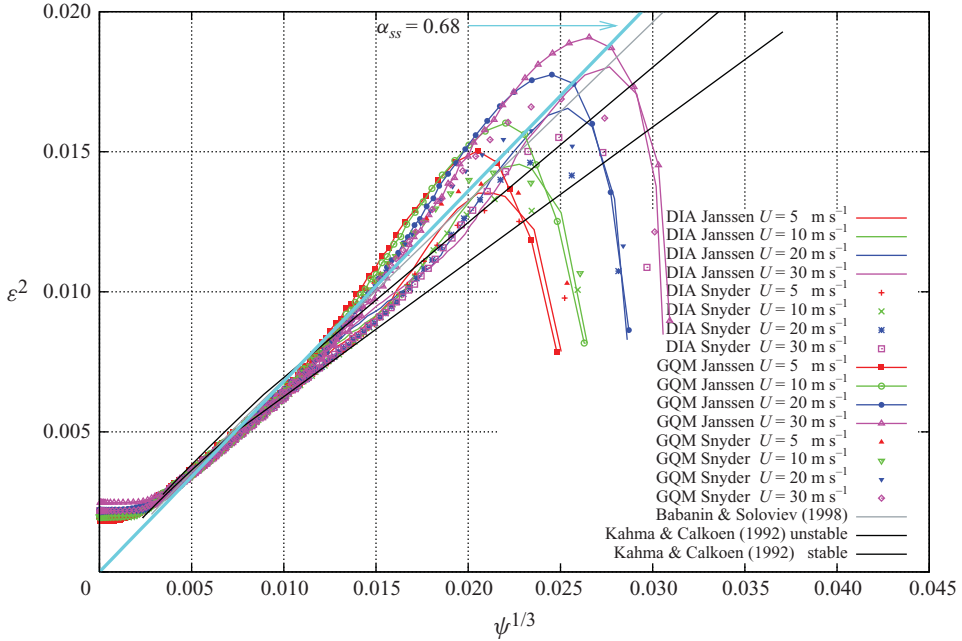


FIGURE 8. Energy-flux dependences in fetch-limited simulations ($\varepsilon^2 = E\omega_p^4/g^2$ versus $\psi^{1/3} = (\omega_p^2/(2g) \times \partial E/\partial x)^{1/3}$). Curves for the four wind speeds, $U_{10} = 5, 10, 20, 30 \text{ m s}^{-1}$, the two parametrizations of the wave input S_{in} (Snyder and Janssen), and DIA and GQM for the S_{nl} computation are superimposed. Comparison with the experimental results of Kahma & Calkoen (1992) and Babanin & Soloviev (1998*b*) is carried out. The light blue curve represents the estimate $\alpha_{ss} = 0.68$.

Figure 9(a) presents ratio α_{ss} for all the numerical runs as a function of wave steepness ε . Figure 9(b) uses a ‘mixed’ representation: the self-similarity parameter α_{ss} of the weakly turbulent approach is plotted as a function of traditional inverse wave age parameter. Higher dispersion of the results in the mixed representation of figure 9 does not look surprising in view of the above discussion.

4.3. Stages of wind-wave growth

The presence of the self-similar stage of wave growth in energy-flux diagrams gives an idea to qualitatively delimit different stages of wave development.

4.3.1. Initial wave growth

Note that wave parameters in figures 8 and 9 start to evolve from right and bottom parts of panels: from maximal non-dimensional wave input, relatively low initial steepness or from maximal inverse wave age. The first points on the right part of figure 8 correspond to non-dimensional fetch $\chi = 2.5$. The wave steepness grows up to a maximum and then starts to decrease for rather short non-dimensional fetch, $\chi \approx 10\text{--}15$. We see strong dispersion of trajectories for different wave input functions, methods for S_{nl} and wind speeds, and no manifestations of self-similar behaviour at this stage. It is useful to specify this stage as the non-self-similar stage of initial wave growth and to define χ^* to be the non-dimensional fetch of the end of this stage. Note the relatively low dispersion of χ^* for different wind speeds, which makes sense for such a demarcation of the initially growing wind-sea stage in terms of conventional

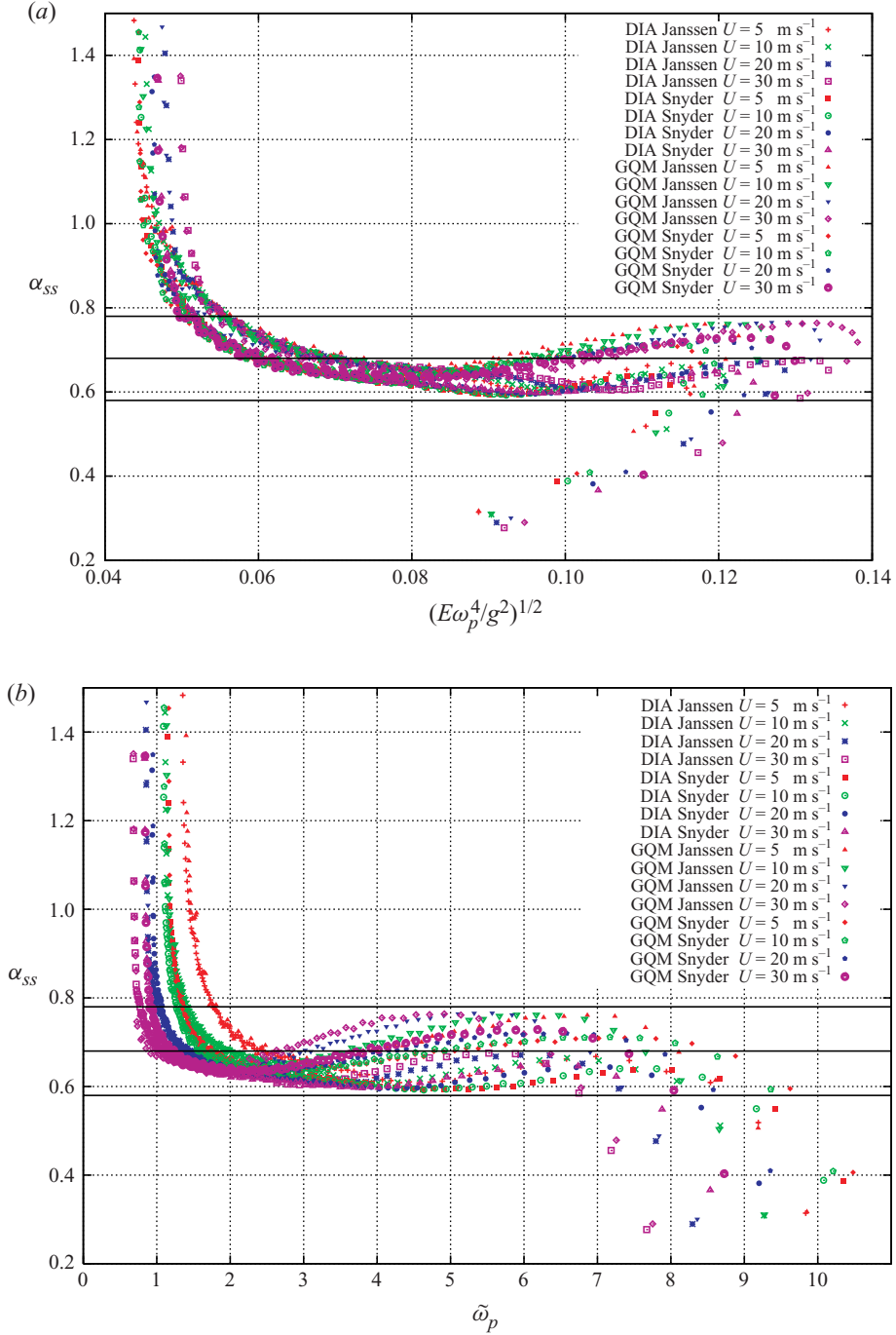


FIGURE 9. Self-similarity parameter α_{ss} as a function of (a) wave steepness $\sqrt{E\omega_p^4/g^2}$ and (b) inverse wave age $\tilde{\omega}_p = U_{10}/C_p$, obtained with wind speeds $U_{10} = 5, 10, 20, 30 \text{ m s}^{-1}$, the two parametrizations of the wave input S_{in} (Snyder and Janssen) and DIA and GQM for the S_{nl} computation. The horizontal lines $\alpha_{ss} = 0.58$, $\alpha_{ss} = 0.68$ and $\alpha_{ss} = 0.78$ are drawn for a better visualization of the estimated coefficient $\alpha_{ss} = 0.68 \pm 0.1$.

wind-speed scaling. In terms of dimensional fetches, this stage is longer for higher winds, which seems counter-intuitive at first glance. With our split-balance model, this ‘detail’ of the full kinetic equation is easy to explain. The self-similar evolution requires nonlinearity to be stronger than wind forcing. At high winds (stronger forcing), it occurs for ‘more strongly nonlinear’ waves with higher steepness and requires longer fetches for the dominance of nonlinearity to be reached.

4.3.2. Self-similar growing wind sea

The maximum of wave steepness is considered as a starting point of the second stage of wave evolution: the growing wind sea stage. This stage is related to the asymptotic split-balance model and the resulting self-similarity features of wind-wave growth.

At the beginning of the stage, the non-self-similar background of the wave spectrum can significantly contaminate inherent features of the self-similar evolution of the wave spectrum. It can explain a slight decrease in the self-similarity parameter α_{ss} with fetch (or wave age). Self-similarity of growing wind sea is manifested by rapid collapsing of trajectories to an asymptotic curve irrespective of particular wave input function and wind speed. At the same time, the dependence on method for S_{nl} is seen clearly: GQM and DIA form two separate bundles of trajectories. These bundles later on merge together. The trajectories for GQM and DIA become remarkably close but the presence of the two bundles is still visible in figure 9(a). The similarity of GQM and DIA results for the growing wind sea is explained quite naturally by homogeneity property (2.9) of the collision integral S_{nl} . Minor deviations are dealing, evidently, with the effect of different shaping of wave spectrum when using GQM or DIA.

The self-similarity parameter α_{ss} again starts to grow slowly when the two bundles in figure 8 collapse to a single one (see figure 9). The latter behaviour appears to be in perfect agreement with the proposed scheme of wave development through a sequence of reference cases of spatial growth (table 1): increase of α_{ss} from $p_\chi = 1$ by Hasselmann *et al.* (1976) to $p_\chi = 3/4$ by Toba (1972) and further to Zakharov & Zaslavsky (1983b) regime ($p_\chi = 4/7$). Thus, one can specify sub-stages of wave evolution within the stage of growing wind sea.

These sub-stages are seen very well in figure 10 with a ‘mixed’ representation of wave steepness (weakly turbulent scale) versus inverse wave age (conventional wind-wave scaling). The three reference curves (reference cases of table 1) show different slopes and fairly good correspondence of these slopes to our simulation results. The gentle slope of the Hasselmann *et al.* (1976) regime is seen as the first sub-stage of growing wind sea (inverse wave age $\tilde{\omega}_p = \omega_p U_{10}/g$ higher than 2.5–3). The Toba (1972) second sub-stage covers a relatively narrow range of inverse wave age 1.5–2.5. The further steepening of trajectories can be treated as a quite short sub-stage by Zakharov & Zaslavsky (1983b) just before reaching mature sea, where inverse wave age $\tilde{\omega}_p$ tends to be constant.

Thus, universality of wind-wave growth in the sense of weakly turbulent theory is demonstrated fairly well at this self-similar stage of wave development. Simulation results show that weakly turbulent scaling is a good and proactive tool for analysis of the physics of growing wind sea.

4.3.3. Mature wind sea

The existence of a limiting wind sea state at infinitely long fetches is an open question (see, for discussion, Komen *et al.* 1984). Here we refer to mature sea as a state of saturation of total energy and spectral peak frequency that is observed

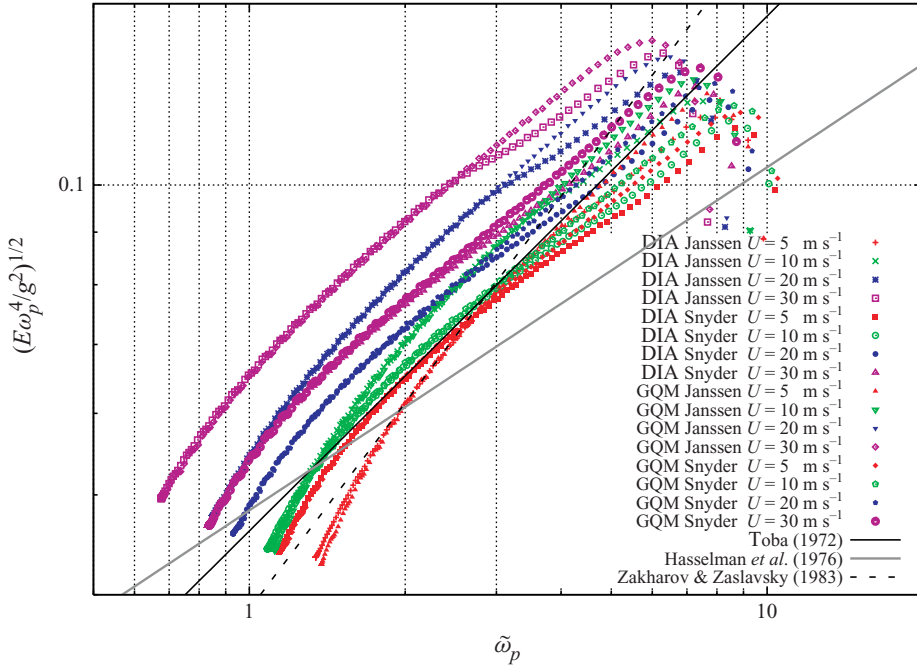


FIGURE 10. Steepness $\sqrt{E\omega_p^4/g^2}$ as a function of inverse wave age $\tilde{\omega}_p = U_{10}/C_p$ in log scale. Reference regimes give tangents 1/3 for Hasselmann, 1/2 for Toba, 2/3 for Zakharov & Zaslavsky.

easily in figures 2 and 3, leaving the question of the existence of the saturated spectral distribution for future studies. In energy-flux plots (figure 8), the mature sea state is identified quite naturally as a pronounced deviation of trajectories above the asymptotic straight line. Wave steepness (ordinate axis) is tending to a limiting value, while net wave input (abscissa) is vanishing. This stage can also be observed easily in figure 9 when inverse wave age and wave steepness asymptotically tend to their limits.

The limiting value of steepness $\varepsilon = \sqrt{E\omega_p^4/g^2}$ depends on the parametrization of wind input and on the wind speed. This is in contrast to the classic case of the Pierson–Moskowitz spectrum (Pierson & Moskowitz 1964) for which steepness has a universal value:

$$\varepsilon_{PM}^2 = \frac{E_{PM}\omega_{PM}^4}{g^2} = \frac{\alpha}{5} \approx 0.0016. \tag{4.4}$$

Here $\alpha = 0.0081$ is the Phillips constant in the Pierson–Moskowitz spectrum. Nevertheless, our results give values $\varepsilon^2 = 0.0018\text{--}0.0024$, which are a bit higher but still close to the Pierson–Moskowitz value, especially for low winds, i.e. wind speeds of 5 and 10 m s⁻¹ ($\varepsilon < 0.002$). Higher winds give ‘more severe’ mature sea with higher steepness ε . Note that dependence of the limiting steepness of mature sea on the method for calculating S_{nl} is very weak.

Quite similarly to the case of initially growing waves, the evolution of mature sea is not self-similar but features of the ‘non-self-similarity’ are perfectly different. All the constituents on the right-hand side of (1.1) appear to be equally important, in contrast to the young sea case where wave input S_{in} is very likely dominating. For

mature sea, the terms S_{in} , S_{diss} , S_{nl} are close in magnitudes. More importantly, terms of input and dissipation reach their extremes in different wave spectral ranges (see e.g. Komen *et al.* 1984, for details). Hence, nonlinear transfer continues to play a key role redistributing wave energy within the wave spectrum. Thus, the problem of mature sea remains an inherently nonlinear problem in contrast to initial growth case which can be referred to as a quasi-linear one.

We should stress that the inverse wave age of mature sea obtained for high winds (20 and 30 m s⁻¹) (figure 9b) is close to the Pierson–Moskowitz value, $(\omega_p U_{10})/g \approx 0.82$. In our opinion, qualitative correspondence of our simulation results with the Pierson–Moskowitz model is of much greater importance than this simple quantitative coincidence: the spectral peak component in mature sea rides faster than wind. It implies that nonlinear transfer is still playing a key role in the mature stage, transferring energy to waves running faster than wind.

5. Discussion and conclusions

In §1, we announced an ambitious goal for this study, namely ‘to present a general vision’ of wave growth, based on our understanding of wind-wave balance. The clue to understanding is the hypothesis of dominating nonlinear transfer. Some arguments for its validity have been given by Badulin *et al.* (2005, 2007) and recently by Zakharov (2009). To use this hypothesis ‘in full’, we have exploited the split-balance model by Badulin *et al.* (2007) and proposed a new approach for wind-wave scaling. We applied the weakly turbulent scaling to a classic problem of wind-wave modelling: fetch-limited growth. Results of simulations gave a basis for discussion of the advantages of the new approach as compared with the traditional scaling suggested by Kitaigorodskii (1962) almost half a century ago.

The proposed weakly turbulent scaling appears to be a powerful tool for physical analysis of the problem. It greatly extends our comprehension of basic features of wind-wave growth. A simple tool of analysis was applied, i.e. the method of energy-flux diagrams that allows us to delimit three stages: (i) the non-self-similar stage of initially growing sea, (ii) the self-similar stage of growing wind sea and (iii) the non-self-similar stage of mature wind waves. Integral characteristics: total energy E , peak frequency ω_p and total wave input dE/dt appear to be quite adequate for this delimitation.

Additionally, the energy-flux analysis allows us to discover finer effects of the methods for modelling wave evolution, say, the rather surprising quality of DIA for the self-similar stage of wave growth. In terms of the weakly turbulent approach, it can be explained easily: both DIA and quasi-exact GQM respect the same homogeneity property (2.9) and, hence, manifest quite close self-similar behaviour. The minor differences in energy-flux trajectories can be partly due to feedback effects of spectral shapes on total wave input (see §4.2.1 and figure 7). Evidently, dependence of total wave input on a particular method of wave modelling is not a good thing. The need to control this important physical quantity is our main recommendation for improving the modelling of wind-wave growth.

The self-similar stage of wind-wave growth, in its turn, can be divided into sub-stages in accordance with reference cases introduced in §§3.3 and 3.4. These cases correspond to constant fluxes of wave momentum, energy and action to waves. It leads us to a consistent scheme of wind-wave interaction where these different regimes of wave growth can be associated with different physical mechanisms of wind-wave coupling.

The first sub-stage of relatively young waves is governed mostly by momentum flux of turbulent wind; the corresponding flux of energy is growing with wave phase speed (the $5/3$ law by Hasselmann *et al.* 1976). The wave momentum flux can be associated quite naturally with momentum flux due to turbulent wind (wind stress). The next sub-stage is associated with the well-known $3/2$ law of Toba (1972) when the energy flux to waves becomes constant. The wave momentum decays with wave growth, which means decay of turbulent wind stress coming to waves. The last reference case of Zakharov & Zaslavsky (1983*b*) gives decay in both wave momentum and wave energy fluxes while wave action flux remains constant. Dependence of total wave input on both external forcing (wind speed) and stage of wave development described by, say, non-dimensional wave age parameter u_* / C_p is quite often taken into account in parametrizations of wave input (see e.g. Resio, Long & Vincent 2004). Our reference cases propose a theoretical background for such parametrizations and determine the link of a particular dependence with a physical mechanism of wave production (due to wind stress, energy flux, etc.).

The extensive numerical study presented in this paper gave us estimates of the key parameter α_{ss} of our asymptotic theory and its dependence on the rate of wave growth p_χ . The estimate $\alpha_{ss}(p_\chi = 3/4) = 0.68$ for the Toba sub-stage of growing sea (or more general approximate dependence $\alpha_{ss}(p_\chi) \approx 0.62 p_\chi^{-1/3}$) appears to be consistent with:

- (i) previous numerical results on duration-limited growth (Badulin *et al.* 2008*a*);
- (ii) wind sea experiments (Badulin *et al.* 2007);
- (iii) wind-wave tank experiments (Badulin & Caulliez 2009).

Further delimitation of sub-stages of self-similar wave growth can be made quantitatively, and not only qualitatively. Figure 10 gives such estimates of wave development stages in terms of ‘mixed’ presentation: steepness (from weakly turbulent scaling) and inverse wave age (from conventional wind-speed scaling). The sub-stage curves (the $5/3$, $3/2$, $4/3$ laws) give remarkable references, first of all, for slopes of simulation curves and, to a lesser extent, for magnitudes. Simulation results show a better consistency with the reference cases for low winds. This looks reasonable as experimental dependences generally correspond to low-to-moderate wind conditions (less than 10 m s^{-1}).

We stress once more that our simulations followed conventional approaches for wind-wave modelling. Thus, key results can be reproduced quite easily, at least with the well-known DIA for S_{nl} . More expensive ‘exact’ methods for evaluating nonlinear transfer are now available in a number of research groups (e.g. Hasselmann & Hasselmann 1981, 1985; Resio & Perrie 1991; Komatsu & Masuda 1996; Polnikov 1997; Hashimoto *et al.* 1998; Lavrenov 2001, 2003; Pushkarev *et al.* 2003; van Vledder 2006) and, in principle, reproduction of our results is feasible in its full.

We see many good opportunities to develop wind-wave studies in the setting of the weakly turbulent approach. Two questions are of primary importance, in our opinion. First, spectral and angular distributions of wave spectrum at different stages of wave development should be studied in more detail. Spectral distributions manifest self-similarity properties only partially (see the discussion of the ‘magic circle’ problem in Badulin *et al.* 2005, §6.1.2). This should be taken into account for correct assessment of their feedback on total wave input. The study of this effect is a very delicate theoretical and numerical problem.

The second question deals with alternative models of wave input (see e.g. Donelan *et al.* 2006; Tsagareli *et al.* 2010) or dissipation (e.g. Young & Babanin 2006; van der Westhuysen *et al.* 2007; Ardhuin *et al.* 2008; Filipot *et al.* 2010). The introduction of these models will very likely not change key results of self-similar stage of wave

growth. If so, it would be an additional stimulus to further develop the ‘general vision’ of wave growth presented in this paper.

The research of S.I.B. was conducted under Russian Foundation for Basic Research, 08-05-00648-a, 08-05-13524-ofi-a, 09-05-13605-ofi-c, 09-05-92501-IK_-a Russian Academy Program ‘Mathematical methods of nonlinear dynamics’ and US Army Corps of Engineers Contract W912HZ-10-P-0176. This support is gratefully acknowledged.

Appendix A. Wave input parametrizations by Snyder *et al.* (1981) and Janssen (1989, 1991)

In this appendix, the main characteristics of the models used for S_m in the present study are recalled briefly. These models share the same form given by (2.5), leading to an exponential growth. For the Snyder *et al.* (1981) input term, the growth rate $\beta(f, \theta)$ in (2.5) is determined by the ratio u_*/C_{ph} only:

$$\beta(f, \theta) = \max \left[0; 0.25 \frac{\rho_a}{\rho_w} \left(28 \frac{u_*}{C_{ph}} \cos(\theta - \theta_w) - 1 \right) \right], \quad (\text{A } 1)$$

where ρ_a, ρ_w are the air and water densities, and θ_w is the local direction of the wind. The friction velocity is related to the wind speed by the drag coefficient

$$C_D = \left(\frac{u_*}{U_{10}} \right)^2, \quad (\text{A } 2)$$

which is assumed to be a linear function of wind speed in our study (WAMDI Group 1988):

$$C_D = \begin{cases} 6.5 \times 10^{-5} U_{10} + 8 \times 10^{-4}, & \text{if } U_{10} \geq 7.5 \text{ m s}^{-1}, \\ 1.2875 \times 10^{-3}, & \text{if } U_{10} < 7.5 \text{ m s}^{-1}. \end{cases} \quad (\text{A } 3)$$

As is seen from (A 1) and (A 2), the threshold speed is close to wind speed U_{10} ($U_{10} = 28u_*$ for $U_{10} < 7.5 \text{ m s}^{-1}$).

Note that the Snyder expression is based on field measurements of weakly forced waves in a narrow range of observed inverse wave ages ($1 < U_{10}/C_{ph} < 3$). Thus, the use of this input term (as well as other empirical parametrizations) is ‘based on extrapolation’ (Snyder *et al.* 1981, figure 26) that can lead, in some cases, to corruption of physics.

The model of wave input by Janssen (1989, 1991) uses more parameters of atmospheric boundary layer. In addition to dependence on ratio u_*/C_{ph} , it introduces dependence on sea roughness parameters. The wave growth rate $\beta(f, \theta)$ in (2.5) reads

$$\beta(f, \theta) = \Gamma \frac{\rho_a}{\rho_w} \left\{ \left[\frac{u_*}{C_{ph}} + z_\alpha \right] \max [\cos(\theta - \theta_w); 0] \right\}^2, \quad (\text{A } 4a)$$

where

$$\Gamma = \frac{\Gamma_m}{\kappa^2} \mu \ln^4 \mu. \quad (\text{A } 4b)$$

Here $\Gamma_m = 1.2$ is fixed by Janssen (1991), $\kappa = 0.41$ is the von Kármán constant for no-slip turbulent boundary layer, $z_\alpha = 0.011$ is constant as in WAM-Cycle 4. Parameter

μ is determined by

$$\mu = \min \left[\frac{gz_0}{C_{ph}^2} \exp \left(\frac{\kappa}{[u_*/C_{ph} + z_\alpha] \cos(\theta - \theta_w)} \right); 1 \right], \quad (\text{A } 4\text{c})$$

where

$$z_0 = \frac{\tilde{z}_0}{\sqrt{1 - \tau_w/\tau_s}} \quad (\text{A } 4\text{d})$$

depends on the ratio of wind stress,

$$\tau_s = \rho_a u_*^2, \quad (\text{A } 4\text{e})$$

and wave-induced stress

$$\tau_w = \left| \iint \rho_w \omega S_{in}(f, \theta) (\cos \theta, \sin \theta) df d\theta \right|. \quad (\text{A } 4\text{f})$$

Here

$$\tilde{z}_0 = \alpha u_*^2 / g, \quad (\text{A } 4\text{g})$$

with the Charnock constant default value $\alpha = 0.01$. Friction velocity u_* , roughness parameter z_0 and τ_s are derived from fixed wind velocity U_{10} in our simulations,

$$U_{10} = \frac{u_*}{\kappa} \ln \left(\frac{10 + z_0 + \tilde{z}_0}{z_0} \right) \approx \frac{u_*}{\kappa} \ln \left(\frac{10}{z_0} \right), \quad (\text{A } 4\text{h})$$

using the iterative method of Newton–Raphson for the equation set (A 4).

Note that the Janssen (1989, 1991) parametrization introduces an additional wind-speed scale u_{z_0} and the corresponding non-dimensional argument $u_1 = u_{z_0}/C_{ph}$ into general expression (2.5),

$$u_1 = \frac{u_{z_0}}{C_{ph}} = \frac{\sqrt{gz_0}}{C_{ph}} = \frac{\sqrt{\alpha}}{(1 - \tau_w/\tau_s)^{1/4}} \frac{u_*}{C_{ph}}, \quad (\text{A } 5)$$

where u_{z_0} is the friction velocity modified by the feedback effect of wave-induced stress τ_w (see (A 4f)) on air flow and, generally, is small in comparison with u_* .

Finally, we mention that the exponential growth term (2.5) for S_{in} has been supplemented by a linear growth term S_{lin} . This term has been added to the source function so that the waves start to grow from a flat sea surface, and its contribution is noticeable only in the very early stage of wave development. We used the model of Cavaleri & Malanotte-Rizzoli (1981), as implemented by Tolman (1992),

$$S_{lin} = 1.5 \times 10^{-3} g^{-2} \{u_* \max[0, \cos(\theta - \theta_w)]\}^4 \exp \left[- \left(\frac{f}{f_{PM}} \right)^{-4} \right], \quad (\text{A } 6)$$

where f_{PM} is the Pierson–Moskowitz frequency,

$$f_{PM} = \frac{1}{2\pi} \frac{g}{28u_*}. \quad (\text{A } 7)$$

A sample comparison of non-dimensional growth rates $S_{in}(f)/(fF(f))$ by Snyder *et al.* (1981) and by Janssen (1989, 1991) as functions of non-dimensional frequency is shown in figure 11 for wind speed $U_{10} = 10 \text{ m s}^{-1}$, at fetch $x = 10 \text{ km}$ and time $t = 18 \text{ h}$. The Snyder parametrization for β is a simple linear dependence on frequency, i.e. on the only non-dimensional ratio of wind-speed scale u_* to wave phase speed C_{ph} . This

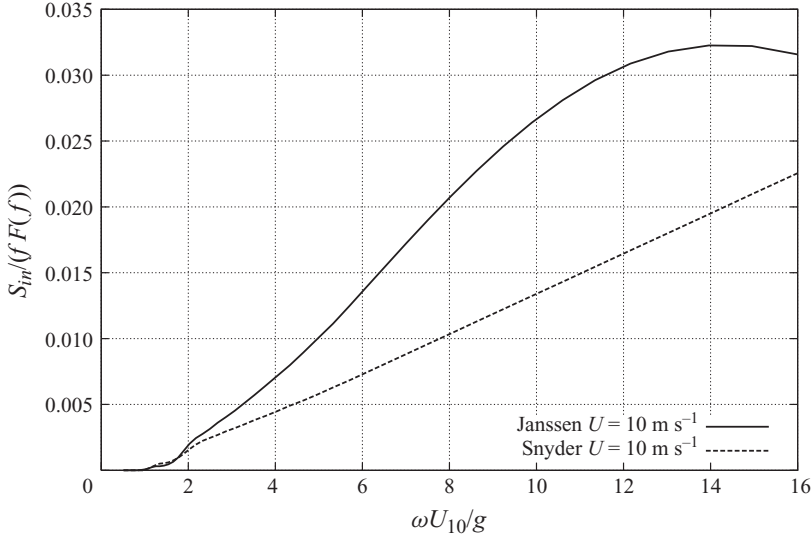


FIGURE 11. Non-dimensional growth rate $S_{in}(f)/(fF(f))$ as a function of the inverse wave age $\omega U_{10}/g$ for parametrizations of the input term S_{in} by Snyder *et al.* (1981) and Janssen (1989, 1991). This figure is obtained from a fetch-limited situation, with wind speed $U_{10} = 10 \text{ m s}^{-1}$, at fetch $x = 10 \text{ km}$ and time $t = 18 \text{ h}$. The DIA method is used in this example to compute S_{nl} .

linear dependence looks quite logical for experimental results obtained in relatively narrow range of wave and wind parameters (see Snyder *et al.* 1981, for details).

The most striking feature of the comparison in figure 11 is that the growth rate $\beta(f)$ by Janssen (1989, 1991) is substantially higher than the one by Snyder *et al.* (1981). This results in considerable difference in integral wave input, and, hence, in resulting wave parameters (total wave energy and characteristic wave frequencies).

Appendix B. Calculation of the S_{nl} term: comparison of CPU times

Calculation of nonlinear transfer term S_{nl} is a very time-consuming part of the simulation of wind-wave growth. The fastest (and less accurate) DIA method takes about 25–30 % of the total simulation time when simulating the Hasselmann equation (1.1) with wind input, dissipation and advection.

It is widely accepted that the use of exact methods dramatically increases the time required to compute the S_{nl} term. For the EXACT-NL of Hasselmann & Hasselmann (1981, 1985) and the method of Webb (1978), for instance, the CPU time of S_{nl} calculation is about 1000 times larger than the DIA CPU time. Recent improvements of the WRT method by Pushkarev *et al.* (2003) and Van Vledder (van Vledder 2006; Bottema & van Vledder 2008) decreased this factor down to a value of 300, which still restricts the use of such methods to specific applications or academic cases.

However, for the simulation of the Hasselmann equation on fetch-limited situations including wind input, dissipation and propagation, the CPU time for GQM with rough resolution (GQM-rough) is only about 25 times larger than the DIA simulation time. This shows that GQM is a valuable candidate for implementation in 3G wave models and could soon be used for practical applications. Calculations with medium resolution require about three times more CPU time than the GQM-rough simulations. Calculations with fine resolution, considered as exact ones, need about 20 times more CPU time than the GQM-rough ones.

REFERENCES

- ALVES, J. H. G. M. & BANNER, M. L. 2003 Performance of a saturation-based dissipation-rate source term in modeling the fetch-limited evolution of wind waves. *J. Phys. Oceanogr.* **33**, 1274–1298.
- ANNENKOV, S. Y. & SHRIRA, V. I. 2006 Role of non-resonant interactions in the evolution of nonlinear random water wave fields. *J. Fluid Mech.* **561**, 181–207.
- ARDHUIN, F., CHAPRON, B. & COLLARD, F. 2009 Observation of swell dissipation across oceans. *Geophys. Res. Lett.* **36**, L06607.
- ARDHUIN, F., COLLARD, F., CHAPRON, B., QUEFFEULOU, P., FILIPOT, J.-F. & HAMON, M. 2008 Spectral wave dissipation based on observations: a global validation. In *Proceedings of Chinese–German Joint Symposium on Hydraulics and Ocean Engineering*, Darmstadt, Germany, pp. 391–400.
- BABANIN, A. N. & SOLOVIEV, Y. P. 1998*a* Field investigation of transformation of the wind wave frequency spectrum with fetch and the stage of development. *J. Phys. Oceanogr.* **28**, 563–576.
- BABANIN, A. N. & SOLOVIEV, Y. P. 1998*b* Variability of directional spectra of wind-generated waves, studied by means of wave staff arrays. *Mar. Freshwater Res.* **49**, 89–101.
- BADULIN, S. I., BABANIN, A. V., RESIO, D. & ZAKHAROV, V. 2007 Weakly turbulent laws of wind-wave growth. *J. Fluid Mech.* **591**, 339–378.
- BADULIN, S. I., BABANIN, A. V., RESIO, D. & ZAKHAROV, V. 2008*a* Numerical verification of weakly turbulent law of wind wave growth. In *Proceedings of the IUTAM Symposium on Hamiltonian Dynamics, Vortex Structures, Turbulence*, Moscow, Russia, 2006 (ed. A. V. Borisov, V. V. Kozlov, I. S. Mamaev & M. A. Sokolovskiy), IUTAM Book Series, vol. 6, pp. 175–190. Springer.
- BADULIN, S. I. & CAULLIEZ, G. 2009 Significance of laboratory observations for modeling wind-driven seas. In *Geophysical Research Abstracts, EGU General Assembly 2009*, vol. 11, EGU2009-12694.
- BADULIN, S. I., KOROTKEVICH, A. O., RESIO, D. & ZAKHAROV, V. E. 2008*b* Wave–wave interactions in wind-driven mixed seas. In *Proceedings of the Rogue Waves 2008 Workshop*, Brest, France (ed. M. Olagnon & M. Prevosto), pp. 77–86. IFREMER.
- BADULIN, S. I., PUSHKAREV, A. N., RESIO, D. & ZAKHAROV, V. E. 2005 Self-similarity of wind-driven seas. *Nonlinear Proc. Geophys.* **12**, 891–946.
- BANNER, M. L., BABANIN, A. V. & YOUNG, I. R. 2000 Breaking probability for dominant waves on the sea surface. *J. Phys. Oceanogr.* **30**, 3145–3160.
- BANNER, M. L. & YOUNG, I. R. 1994 Modeling spectral dissipation in the evolution of wind waves. Part I. Assessment of existing model performance. *J. Phys. Oceanogr.* **24**, 1550–1570.
- BENOIT, M. 2005 Evaluation of methods to compute the non-linear quadruplet interactions for deep-water wave spectra. In *5th International Symposium on Ocean Wave Measurement and Analysis (WAVES'2005)*, Madrid, Spain, Paper 52.
- BENOIT, M. 2006 Implementation and test of improved methods for evaluation of nonlinear quadruplet interactions in a third generation wave model. In *Proceedings of the 30th International Conference on Coastal Engineering*, San Diego, CA, pp. 526–538.
- BENOIT, M. & GAGNAIRE-RENOU, E. 2007 Interactions vague–vague non-linéaires et spectre d'équilibre pour les vagues de gravité en grande profondeur d'eau. In *Proceedings of the 18th Congrès Français de Mécanique*, Grenoble, France (in French).
- BENOIT, M., MARCOS, F. & BECQ, F. 1996 Development of a third generation shallow-water wave model with unstructured spatial meshing. In *Proceedings of the 25th International Conference on Coastal Engineering*, Orlando, FL, pp. 465–478.
- BOOIJ, N., RIS, R. C. & HOLTHUIJSEN, L. H. 1999 A third-generation wave model for coastal regions. Part I. Model description and validation. *J. Geophys. Res.* **104** (C4), 7649–7666.
- BOTTEMA, M. & VAN VLEDDER, G. P. 2008 Effective fetch and non-linear four-wave interactions during wave growth in slanting fetch conditions. *Coast. Engng* **55**, 261–275.
- CAVALERI, L., ALVES, J.-H. G. M., ARDHUIN, F., BABANIN, A., BANNER, M., BELIBASSAKIS, K., BENOIT, M., DONELAN, M., GROENEWEG, J., HERBERS, T. H. C., HWANG, P., JANSSEN, P. A. E. M., JANSSEN, T., LAVRENOV, I. V., MAGNE, R., MONBALIU, J., ONORATO, M., POLNIKOV, V., RESIO, D., ROGERS, W. E., SHEREMET, A., MCKEE SMITH, J., TOLMAN, H. L., VAN VLEDDER, G., WOLF, J. & YOUNG, I. 2007 Wave modelling: the state of the art. *Program. Ocean.* **75**, 603–674.
- CAVALERI, L. & MALANOTTE-RIZZOLI, P. 1981 Wind wave prediction in shallow water: theory and applications. *J. Geophys. Res.* **86** (C5), 10961–10975.

- DONELAN, M. A., BABANIN, A. V., YOUNG, I. R. & BANNER, M. L. 2006 Wave-follower field measurements of the wind-input spectral function. Part II. Parameterization of the wind input. *J. Phys. Oceanogr.* **36**, 1672–1679.
- DONELAN, M. A. & PIERSON JR, W. J. 1987 Radar scattering and equilibrium ranges in wind-generated waves with application to scatterometry. *J. Geophys. Res.* **92** (C5), 4971–5029.
- DONELAN, M. A., SKAFEL, M., GRABER, H., LIU, P., SCHWAB, D. & VENKATESH, S. 1992 On the growth rate of wind-generated waves. *Atmos. Ocean* **30** (3), 457–478.
- FILIPOT, J.-F., ARDHUIN, F. & BABANIN, A. V. 2010 A unified deep-to-shallow water wave-breaking probability parameterization. *J. Geophys. Res.* **115**, C04022.
- GAGNAIRE-RENOU, E., BENOIT, M. & FORGET, P. 2010 Ocean wave spectrum properties as derived from quasi-exact computations of nonlinear wave-wave interactions. *J. Geophys. Res.* (in press), doi:10.1029/2009JC005665.
- GÜNTHER, H., HASSELMANN, S. & JANSSEN, P. A. E. M. 1992 The WAM model Cycle 4 (revised version). *Tech Rep.* 4. Deutsch. Klimatol. Rechenzentrum, Hamburg, Germany.
- HARA, T. & BELCHER, S. E. 2002 Wind forcing in the equilibrium range of wind-wave spectra. *J. Fluid Mech.* **470**, 223–245.
- HASHIMOTO, N., TSURUYA, H. & NAKAGAWA, Y. 1998 Numerical computations of the nonlinear energy transfer of gravity-wave spectra in finite water depths. *Coast. Engng J.* **40**, 23–40.
- HASSELMANN, D. E., DUNKEL, M. & EWING, J. A. 1980 Directional wave spectra observed during JONSWAP 1973. *J. Phys. Oceanogr.* **10**, 1264–1280.
- HASSELMANN, K. 1962 On the nonlinear energy transfer in a gravity wave spectrum. Part 1. General theory. *J. Fluid Mech.* **12**, 481–500.
- HASSELMANN, K. 1974 On the spectral dissipation of ocean waves due to white capping. *Boundary-Layer Meteorol.* **6**, 107–127.
- HASSELMANN, K., ROSS, D. B., MÜLLER, P. & SELL, W. 1976 A parametric wave prediction model. *J. Phys. Oceanogr.* **6**, 200–228.
- HASSELMANN, S. & HASSELMANN, K. 1981 A symmetrical method of computing the nonlinear transfer in a gravity wave spectrum. *Hamburger Geophysikalische Einzelschriften, Reihe A, Heft 52*, Max-Planck-Institut für Meteorologie, 138pp.
- HASSELMANN, S. & HASSELMANN, K. 1985 Computations and parametrizations of the nonlinear energy transfer in a gravity-wave spectrum. Part I. A new method for efficient computations of the exact nonlinear transfer integral. *J. Phys. Oceanogr.* **15**, 1369–1377.
- HASSELMANN, S., HASSELMANN, K., ALLENDER, J. H. & BARNETT, T. P. 1985 Computations and parametrizations of the nonlinear energy transfer in a gravity-wave spectrum. Part II. Parameterizations of the nonlinear energy transfer for application in wave models. *J. Phys. Oceanogr.* **15**, 1378–1391.
- HERSBACH, H. & JANSSEN, P. A. E. M. 1999 Improvement of the short-fetch behavior in the wave ocean model (WAM). *J. Atmos. Ocean. Tech.* **16**, 884–892.
- HSIAO, S. V. & SHEMDIN, O. H. 1983 Measurements of wind velocity and pressure with a wave follower during MARSEN. *J. Geophys. Res.* **88** (C14), 9841–9849.
- JANSSEN, P. A. E. M. 1989 Wave-induced stress and the drag of air flow over sea waves. *J. Phys. Oceanogr.* **19**, 745–754.
- JANSSEN, P. A. E. M. 1991 Quasi-linear theory of wind-wave generation applied to wave forecasting. *J. Phys. Oceanogr.* **21**, 1631–1642.
- KAHMA, K. K. & CALKOEN, C. J. 1992 Reconciling discrepancies in the observed growth of wind-generated waves. *J. Phys. Oceanogr.* **22**, 1389–1405.
- KITAIGORODSKII, S. A. 1962 Applications of the theory of similarity to the analysis of wind-generated wave motion as a stochastic process. *Bull. Acad. Sci. USSR, Geophys. Ser., Engl. Transl.* **N1**, 105–117.
- KITAIGORODSKII, S. A. 1983 On the theory of the equilibrium range in the spectrum of wind-generated gravity waves. *J. Phys. Oceanogr.* **13**, 816–827.
- KOMATSU, K. & MASUDA, A. 1996 A new scheme of nonlinear energy transfer among wind waves: RIAM method. Algorithm and performance. *J. Oceanogr. Soc. Japan* **52**, 509–537.
- KOMEN, G. J., CAVALERI, L., DONELAN, M., HASSELMANN, K., HASSELMANN, S. & JANSSEN, P. A. E. M. 1994 *Dynamics and Modelling of Ocean Waves*. Cambridge University Press.
- KOMEN, G. J., HASSELMANN, S. & HASSELMANN, K. 1984 On the existence of a fully developed wind-sea spectrum. *J. Phys. Oceanogr.* **14**, 1271–1285.

- KOROTKEVICH, A. O., PUSHKAREV, A. N., RESIO, D. & ZAKHAROV, V. E. 2008 Numerical verification of the weak turbulent model for swell evolution. *Eur. J. Mech. B Fluids* **27**, 361–387.
- KRASITSKII, V. P. 1994 On reduced Hamiltonian equations in the nonlinear theory of water surface waves. *J. Fluid Mech.* **272**, 1–20.
- LAVRENOV, I. V. 2001 Effect of wind wave parameter fluctuation on the nonlinear spectrum evolution. *J. Phys. Oceanogr.* **31**, 861–873.
- LAVRENOV, I. V. 2003 *Wind-Waves in Oceans: Dynamics and Numerical Simulations*. Springer.
- MASUDA, A. 1986 Nonlinear energy transfer between random gravity waves. In *Waves Dynamics and Radio Probing of the Ocean Surface* (ed. O. Phillips & K. Hasselmann), pp. 136–149. Plenum Press.
- PETERSSON, H. 2004 Wave growth in a narrow bay. PhD thesis, University of Helsinki, Helsinki, Finland.
- PHILLIPS, O. M. 1981 The dispersion of short wavelets in the presence of a dominant long wave. *J. Fluid Mech.* **107**, 465–485.
- PHILLIPS, O. M. 1985 Spectral and statistical properties of the equilibrium range in wind-generated gravity waves. *J. Fluid Mech.* **156**, 505–531.
- PIERSON, W. J. & MOSKOWITZ, L. A. 1964 A proposed spectral form for fully developed wind seas based on the similarity theory of S. A. Kitaigorodskii. *J. Geophys. Res.* **69**, 5181–5190.
- PLANT, W. J. 1982 A relationship between wind stress and wave slope. *J. Geophys. Res.* **87** (C3), 1961–1967.
- POLNIKOV, V. G. 1990 Numerical solution of the kinetic equation for surface gravity waves. *Izv. Atmos. Ocean. Phys.* **26** (2), 168–176.
- POLNIKOV, V. G. 1997 Nonlinear energy transfer through the spectrum of gravity waves for the finite depth case. *J. Phys. Oceanogr.* **27**, 1481–1491.
- PUSHKAREV, A. N., RESIO, D. & ZAKHAROV, V. E. 2003 Weak turbulent theory of the wind-generated gravity sea waves. *Phys. D Nonlinear Phenom.* **184**, 29–63.
- RESIO, D. T., LONG, C. E. & VINCENT, C. L. 2004 Equilibrium-range constant in wind-generated wave spectra. *J. Geophys. Res.* **109**, C01018.
- RESIO, D. T. & PERRIE, W. 1991 A numerical study of nonlinear energy fluxes due to wave–wind interactions. *J. Fluid Mech.* **223**, 603–629.
- SNYDER, R. L., DOBSON, F. W., ELLIOT, J. A. & LONG, R. B. 1981 Array measurements of atmospheric pressure fluctuations above surface gravity waves. *J. Fluid Mech.* **102**, 1–59.
- STEWART, R. W. 1974 The air–sea momentum exchange. *Boundary-Layer Meteorol.* **6**, 151–167.
- SWAMP GROUP 1985 *Ocean Wave Modelling*. Plenum Press.
- TOBA, Y. 1972 Local balance in the air–sea boundary processes. Part I. On the growth process of wind waves. *J. Oceanogr. Soc. Japan* **28**, 109–121.
- TOBA, Y. 1978 Stochastic form of the growth of wind waves in a single-parameter representation with physical implementations. *J. Phys. Oceanogr.* **8**, 494–507.
- TOBA, Y. 1997 Wind-wave strong wave interactions and quasi-local equilibrium between wind and wind sea with the friction velocity proportionality. In *Nonlinear Ocean Waves* (ed. W. Perrie), *Advances in Fluid Mechanics*, vol. 17, pp. 1–59. Computational Mechanics Publications.
- TOLMAN, H. L. 1991 A third generation model for wind on slowly varying, unsteady and inhomogeneous depth and currents. *J. Phys. Oceanogr.* **21**, 766–781.
- TOLMAN, H. L. 1992 Effects of numerics on the physics in a third-generation wind-wave model. *J. Phys. Oceanogr.* **22**, 1095–1111.
- TOLMAN, H. L. 2002 User manual and system documentation of WAVEWATCH-III version 2.22. *Tech Rep. 222*. NOAA/NWS/NCEP/MMAB.
- TOLMAN, H. L. 2004 Inverse modeling of discrete interaction approximations for nonlinear interactions in wind waves. *Ocean Model.* **6**, 405–422.
- TRACY, B. & RESIO, D. 1982 Theory and calculation of the nonlinear energy transfer between sea waves in deep water. *WES Rep. 11*. US Army, Engineer Waterways Experiment Station.
- TSAGARALI, K. N., BABANIN, A. V., WALKER, D. J. & YOUNG, I. R. 2010 Numerical investigation of spectral evolution of wind waves. Part I. Wind-input source function. *J. Phys. Oceanogr.* **40**, 656–666.
- VAN VLEDDER, G. P. 2006 The WRT method for the computation of non-linear four-wave interactions in discrete spectral wave models. *Coastal Engng* **53**, 223–242.

- WAMDI GROUP 1988 The WAM model: a third generation ocean wave prediction model. *J. Phys. Oceanogr.* **18**, 1775–1810.
- WEBB, D. J. 1978 Non-linear transfers between sea waves. *Deep Sea Res.* **25**, 279–298.
- VAN DER WESTHUYSEN, A. J., ZIJLEMA, M. & BATTJES, J. A. 2007 Nonlinear saturation-based whitecapping dissipation in SWAN for deep and shallow water. *Coastal Engng* **454**, 151–170.
- YOUNG, I. R. 2006 Directional spectra of hurricane wind waves. *J. Geophys. Res.* **111**, C08020.
- YOUNG, I. R. & BABANIN, A. V. 2006 Spectral distribution of energy dissipation of wind-generated waves due to dominant wave breaking. *J. Phys. Oceanogr.* **36**, 376–394.
- YOUNG, I. R., HASSELMANN, S. & HASSELMANN, K. 1987 Computations of the response of a wave spectrum to a sudden change in the wind direction. *J. Phys. Oceanogr.* **17**, 1317–1338.
- YOUNG, I. R. & VAN VLEDDER, G. 1993 A review of the central role of nonlinear interactions in wind-wave evolution. *Phil. Trans. R. Soc. Lond.* **342**, 505–524.
- ZAKHAROV, V. E. 1966 Problems of the theory of nonlinear surface waves. PhD thesis, Budker Institute for Nuclear Physics, Novosibirsk, Russia.
- ZAKHAROV, V. E. 1999 Statistical theory of gravity and capillary waves on the surface of a finite-depth fluid. *Eur. J. Mech. B Fluids* **18**, 327–344.
- ZAKHAROV, V. E. 2009 On domination of nonlinear wave interaction in the energy balance of wind-driven sea. In *Proceedings of the 11th International Workshop on Wave Hindcasting and Forecasting*, Halifax, Canada, 2009.
- ZAKHAROV, V. E., FALKOVICH, G. & LVOV, V. 1992 *Kolmogorov Spectra of Turbulence. Part I*. Springer.
- ZAKHAROV, V. E. & FILONENKO, N. N. 1966 Energy spectrum for stochastic oscillations of the surface of a fluid. *Sov. Phys. Dokl.* **160**, 1292–1295.
- ZAKHAROV, V. E., KOROTKEVICH, A. O., PUSHKAREV, A. N. & RESIO, D. 2007 Coexistence of weak and strong wave turbulence in a swell propagation. *Phys. Rev. Lett.* **99** (164501).
- ZAKHAROV, V. E. & ZASLAVSKY, M. M. 1982a Kinetic equation and Kolmogorov spectra in the weak-turbulence theory of wind waves. *Izv. Atmos. Ocean. Phys.* **18** (9), 970–980.
- ZAKHAROV, V. E. & ZASLAVSKY, M. M. 1982b Integrals of input and dissipation in the weak-turbulence theory of wind-generated waves. *Izv. Atmos. Ocean. Phys.* **18** (10), 1066–1076.
- ZAKHAROV, V. E. & ZASLAVSKY, M. M. 1983a Shape of spectrum of energy carrying components of a water surface in the weak-turbulence theory of wind waves. *Izv. Atmos. Ocean. Phys.* **19** (3), 207–212.
- ZAKHAROV, V. E. & ZASLAVSKY, M. M. 1983b Dependence of wave parameters on the wind velocity, duration of its action and fetch in the weak-turbulence theory of water waves. *Izv. Atmos. Ocean. Phys.* **19** (4), 300–306.
- ZASLAVSKY, M. M. 1984 Wind-wave forecasting as a problem of the weak turbulence theory. Doctor of Science thesis, P. P. Shirshov Institute of Oceanology of the Academy of Sciences of the USSR, Moscow, Russia (in Russian).